



HAL
open science

Ozone and carbon monoxide budgets over the Eastern Mediterranean

S. Myriokefalitakis, Nikolaos Daskalakis, G.S. Fanourgakis, A. Voulgarakis, M.C. Krol, J.M.J. Aan de Brugh, M. Kanakidou

► **To cite this version:**

S. Myriokefalitakis, Nikolaos Daskalakis, G.S. Fanourgakis, A. Voulgarakis, M.C. Krol, et al.. Ozone and carbon monoxide budgets over the Eastern Mediterranean. *Science of the Total Environment*, 2016, 563-564, pp.40-52. 10.1016/j.scitotenv.2016.04.061 . insu-01330364

HAL Id: insu-01330364

<https://insu.hal.science/insu-01330364v1>

Submitted on 4 Mar 2021

HAL is a multi-disciplinary open access archive for the deposit and dissemination of scientific research documents, whether they are published or not. The documents may come from teaching and research institutions in France or abroad, or from public or private research centers.

L'archive ouverte pluridisciplinaire **HAL**, est destinée au dépôt et à la diffusion de documents scientifiques de niveau recherche, publiés ou non, émanant des établissements d'enseignement et de recherche français ou étrangers, des laboratoires publics ou privés.

1 **Ozone and carbon monoxide budgets over the Eastern**
2 **Mediterranean**

3 **S. Myriokefalitakis ^a, N. Daskalakis ^{a,b,1}, G. S. Fanourgakis ^a, A. Voulgarakis ^c, M. C. Krol**
4 **^{d,e,f}, J. M. J. Aan de Brugh ^f and M. Kanakidou ^a**

5 ^a Environmental Chemical Processes Laboratory (ECPL), Department of Chemistry, University
6 of Crete, P.O. Box 2208, 70013 Heraklion, Greece

7 ^b Institute of Chemical Engineering, Foundation for Research and Technology Hellas
8 (FORTH/ICE - HT), 26504 Patras, Greece

9 ^c Department of Physics, Imperial College London, London, UK

10 ^d Meteorology and Air Quality Section, Wageningen University, Wageningen, The Netherlands

11 ^e Institute for Marine and Atmospheric Research, Utrecht University, Utrecht, The Netherlands

12 ^f SRON Netherlands Institute for Space Research, Utrecht, The Netherlands

13 ¹now at: LATMOS, Laboratoire Atmosphères, Milieux, Observations Spatiales,
14 UPMC/UVSQ/CNRS, Paris, France

15

16 Corresponding author: stelios@uoc.gr (S. Myriokefalitakis); mariak@uoc.gr (M. Kanakidou)

17

18 **Abstract**

19 The importance of the long-range transport (LRT) on O₃ and CO budgets over the Eastern
20 Mediterranean has been investigated using the state-of-the-art 3-dimensional global chemistry-
21 transport model TM4-ECPL. A 3-D budget analysis has been performed separating the Eastern
22 from the Western basins and the boundary layer (BL) from the free troposphere (FT). The FT of
23 the Eastern Mediterranean is shown to be a strong receptor of polluted air masses from the
24 Western Mediterranean, and the most important source of polluted air masses for the Eastern
25 Mediterranean BL, with about 40% of O₃ and of CO in the BL to be transported from the FT
26 aloft. Regional anthropogenic sources are found to have relatively small impact on regional air
27 quality in the area, contributing by about 8% and 18% to surface levels of O₃ and CO,
28 respectively. Projections using anthropogenic emissions for the year 2050 but neglecting climate
29 change calculate a surface O₃ decrease of about 11% together with a surface CO increase of
30 roughly 10% in the Eastern Mediterranean.

31 **Keywords:** Ozone (O₃), Carbon monoxide (CO), Eastern Mediterranean (EM), Long-range
32 transport (LRT), Free Troposphere (FT)

33

34 **1. Introduction**

35 Tropospheric O₃ and CO are atmospheric pollutants both generated from natural and
36 anthropogenic sources depending on numerous physical and chemical processes (e.g. Lelieveld
37 and Dentener, 2000). They significantly affect the oxidizing capacity of the troposphere, climate
38 (IPCC, 2013) and human and ecosystem's health (e.g. Jimoda, 2012; Ainsworth et al., 2012; Yue
39 and Unger, 2014). Therefore, much attention is been paid to limit exceedances of threshold air
40 pollution levels set by Environmental policy directives (e.g. DIRECTIVE 2008/50/EC Annex
41 VII). Attribution of air pollution to sources is a prerequisite for designing measures to be taken to
42 comply with such instructions. Pollution within urban agglomerations can build-up both locally
43 (via local emissions and chemistry) and regionally (via transport from other regions) (e.g. Parrish
44 et al., 2011). In the outflow of pollution centers, oxidation of volatile organic compounds
45 (VOCs) and CO fosters the formation of secondary pollutants such as O₃ (Molina and Molina,
46 2002), which is produced during the oxidation of VOCs in the presence of nitrogen oxides (NO_x)
47 (Crutzen, 1974; Derwent et al., 1996; Monks et al., 2009) following non-linear chemical
48 processes. Therefore, it is particularly important to know whether actions on national level or
49 coordinated actions on regional, or even global scale, are needed to limit air pollution in a region.

50 In this respect, Colette et al. (2012) analyzed atmospheric pollutant surface observations in
51 Europe to derive trends over the past decade and compared them with multi-model chemistry-
52 transport simulations. They found robust decreases of NO_x throughout Europe except in South-
53 Eastern France and North Italy and pointed out much larger model uncertainty over the
54 Mediterranean than elsewhere. Over the Eastern Mediterranean (EM), they calculate a decrease
55 in non-methane volatile organic compounds (NMVOC) to NO_x ratio indicating a shift in the
56 chemical regime in the area. Beekmann and Vautard (2010) have shown that the Mediterranean
57 atmosphere is a NO_x sensitive regime, while North-Western Europe is always VOC sensitive.
58 Furthermore, modeling studies simulate high O₃ concentrations in the summer, in agreement
59 with the observed northern hemisphere summertime O₃ maxima (Zanis et al., 2014). They also
60 predict higher O₃ levels in parts of the European continent as a result of a warmer climate in the
61 near future (Langner et al., 2012; Zanis et al., 2014) and an increase in regional biogenic
62 emissions, both of which lead to a summertime regional O₃ increase by 1 ppb °C⁻¹ (Im et al.,
63 2011). Within large agglomerations of the EM, O₃ is significantly depressed through reaction

64 with NO, followed by HNO₃ formation, in particular during wintertime (Im and Kanakidou,
65 2012).

66 The Mediterranean is among the most climatically sensitive regions of Europe, often exposed to
67 multiple stresses, such as simultaneous water shortage and air pollution exposure (IPCC, 2013).
68 It is also a characteristic region of a strongly coupled atmosphere-ocean system, composed by
69 two basins that differ in air circulation patterns (Millán et al., 2005; Kallos et al., 2007) – the
70 eastern and the western part. EM is affected by several large agglomerations, including the two
71 megacities (<http://www.newgeography.com>): Istanbul (13.6 M; Turkey) at the northeastern edge,
72 Cairo (17.8 M; Egypt) at the southern edge of the basin, and one agglomeration, Athens, which
73 gathers 40% (4 M) of Greece's total population. The rapid urbanization and the unique location
74 of the EM as a cross-road of air masses affected by various pollution sources has turned air
75 pollution into a challenging environmental problem in the area. Air masses from upwind
76 locations carrying anthropogenic emissions, mainly from Europe, the Balkans and the Black Sea,
77 meet with biomass burning (Sciare et al., 2008), biogenic (Liakakou et al., 2009) and other
78 natural emissions (Gerasopoulos et al., 2011) from surrounding regions under sunny and warm
79 conditions that enhance photochemical build-up of pollutants (Lelieveld et al., 2002; Kanakidou
80 et al., 2011).

81 To quantify the impact of anthropogenic sources on air-quality of the region as the EM, the inter-
82 and the intra- continental transport have to be considered and distinguished from the impact of
83 the regional sources (HTAP, 2011). Such analysis remains challenging, due to the chemical
84 complexity of atmospheric composition and the significant seasonal and interannual variability
85 of meteorological conditions that affect transport patterns (e.g. driven by the North Atlantic
86 Oscillation; Pausata et al., 2012). Thus, large-scale chemistry-transport models (CTMs) are more
87 appropriate tools for studying LRT (e.g. HTAP, 2011) than mesoscale models in which inter-
88 /intra-continental transport procedures are strongly driven by the imposed boundary conditions.
89 Satellite observations of tropospheric O₃, NO₂ and aerosol optical thickness (AOT) over the
90 Mediterranean clearly show the regional tropospheric O₃ column maximum over the
91 Mediterranean sea as well as the high NO₂ columns in the urban pollution centers that surround
92 the basin (Kanakidou et al., 2011). Ground-based and satellite observations and numerical
93 modeling reviewed by Kanakidou et al. (2011) point out that air pollution transported to the area
94 is of similar importance to local sources for the background air pollution levels in the EM.

95 Indeed, Drori et al. (2012) calculated that transport of air masses from Eastern Europe and
96 Turkey to the EM can contribute up to 50 % of surface CO in the area. Gerasopoulos et al.
97 (2005) analyzing observations provided evidence that the main mechanism controlling the high
98 background tropospheric O₃ levels in the EM is the long-range transport (LRT) from the
99 European continent (mainly during summer) and the local photochemical O₃ build-up (especially
100 under western flow and stagnant wind conditions). In line with these findings, Zanis et al. (2014)
101 attributed the characteristic summertime tropospheric O₃ pool over the EM to enhanced
102 downward transport from the upper troposphere and lower stratosphere that characterize the
103 summertime circulation over this region.

104 In the present study we investigate the contribution of LRT on O₃ and CO budgets in the
105 Mediterranean basin, using a global CTM, the TM4-ECPL, to conduct a source attribution of
106 atmospheric composition changes. The relative impacts of regional anthropogenic, biomass
107 burning and natural emissions to the air quality in the EM are evaluated. First, the model set-up
108 and methodology followed are described. Then simulated O₃ and CO levels are compared with
109 in-situ observations and satellite retrievals on a European and global level and model
110 deficiencies are discussed. The importance of regional emissions and the strength of LRT for air
111 quality are investigated based on sensitivity simulations and budget analysis. Projected changes
112 resulting from anthropogenic emissions scenarios for 2050 are also discussed.

113 **2. Materials and Methods**

114 *2.1 Global Model Set-up*

115 The global CTM TM4-ECPL (Daskalakis et al., 2015 and references therein) is able to simulate
116 oxidant chemistry, accounting for NMVOCs, as well as all major aerosol components, including
117 inorganic aerosols such as sulfate (SO₄²⁻), nitrate (NO₃⁻), ammonium (NH₄⁺) using the
118 ISORROPIA II thermodynamic model (Fountoukis and Nenes, 2007) and secondary organic
119 aerosols (SOA). Compared to its parent TM4 model (van Noije et al., 2004), the present version
120 includes a description of glyoxal and other oxygenated organics (Myriokefalitakis et al., 2008)
121 and organic aerosols (Myriokefalitakis et al., 2010). The model also accounts for multiphase
122 chemistry in clouds and aerosol water that affects SOA formation (Myriokefalitakis et al., 2011)
123 and dust solubility (Myriokefalitakis et al., 2015). TM4-ECPL has been previously evaluated for
124 its ability i) to compute atmospheric composition and uncertainties associated with the use of

125 different biomass burning emissions (Daskalakis et al., 2015), ii) to reproduce distributions of
126 tropospheric O₃ and its precursors, as well as aerosols over Asia in summer 2008 as seen by
127 satellite and by in-situ observations (Quennehen et al., 2015), iii) to simulate the concentrations
128 of sulfate, black carbon (BC) and other aerosols in the Arctic (Eckhardt et al., 2015) and iv) to
129 evaluate the air quality impacts of short-lived pollutants based on current legislation for the
130 recent past and present (Stohl et al., 2015).

131 For the present study, year 2008 anthropogenic emissions of NMVOC, NO_x, CO, SO₂, NH₃, OC
132 and BC developed within the EU - FP7 ECLIPSE project (Stohl et al., 2015) have been used to
133 drive the chemistry in the model. Methane (CH₄) is calculated by nudging surface concentrations
134 to NOAA flask observations representative of the year of simulation (currently available for the
135 years 1989-2010; M. van Weele, personal communication, 2013). Since TM4-ECPL does not
136 explicitly calculate stratospheric chemistry, upper boundary conditions derived from climatology
137 records of stratospheric concentrations have been applied for O₃, CH₄ and HNO₃. Thus,
138 stratospheric O₃ concentrations are nudged above 50hPa to the concentrations of the year of
139 simulation based on the Multi-Sensor Reanalysis (MSR) climatology record, which is available
140 for the years 1978-2008 (van der A et al., 2010). For stratospheric CH₄ concentrations, the
141 monthly climatology based on the HALogen Occultation Experiment (HALOE) on board the
142 Upper Atmosphere Research Satellite (UARS) (Groß and Russell III, 2005) is applied above 50
143 hPa. In the stratosphere, HNO₃ is nudged at 10 hPa using Sub-millimetre and Millimetre
144 Radiometer (SMR) observations from the Odin satellite (Brohede et al., 2008). This approach
145 enables a realistic representation of the concentrations of these compounds in the upper layers of
146 the model and thus of the vertical exchanges between the stratosphere and the troposphere.
147 Further detailed information on the model set up and the emission inventories used in the model
148 is available in Daskalakis et al. (2015).

149 Here, TM4-ECPL is driven by ECMWF (European Center for Medium - Range Weather
150 Forecasts) Interim re-analysis project (ERA-Interim) meteorology (Dee et al., 2011). Advection
151 of the tracers in the model is parameterized using the slopes scheme (Russell and Lerner, 1981).
152 Convective transport is parameterized based on the Tiedtke (1989) and Olivié (2004) scheme.
153 The vertical diffusion is parameterized as described in Louis (1979). The basic model
154 configuration used for this study (BASE simulation; see Table 1) has a horizontal resolution of
155 3° in longitude by 2° in latitude, 34 vertical hybrid layers from the surface up to 0.1 hPa and a

156 time-step of 30 min. For this work, all simulations were performed using meteorology for the
157 year 2008. A spin-up of one year (i.e. for the year 2007) with the respective meteorology and
158 emissions has been applied.

159 *2.2 Simulations and Emission Perturbations*

160 A number of simulations have been further performed for this study (Table 1) in order to
161 investigate the importance of LRT over the Mediterranean basin, focusing in particular on the
162 EM part. In short, simulations are performed to investigate the impact of regional anthropogenic
163 (MaskANTHRO), biogenic (MaskBIO) and biomass burning (MaskBB) emissions in the EM.
164 The simulation MaskALL neglects all regional emissions to provide information on the
165 background air-quality levels (sustained by mid - and long - range transport to the EM). Note
166 that for the present work, the area between 15°E - 40°E in longitude and 30°N - 45°N in latitude
167 is defined as the EM domain in the model (i.e. 25 longitudinal boxes and 15 latitudinal boxes for
168 the BASE simulation).

169 Additionally, simulations are performed to separately investigate the impact of LTR from non-
170 EM parts of Europe (MaskEU), North America (MaskNAM), Asia (MaskAS) and Africa
171 (MaskAF) to the EM background atmosphere. For this work, we use the HTAP phase 2
172 definitions (available online via the HTAP Wiki-page) for the source regions over which
173 emissions are masked. An additional simulation (FUTURE) investigates the impact of future
174 global anthropogenic emissions on EM O₃ levels, based on emission projections for the year
175 2050 (Stohl et al., 2015). The sensitivity simulations for the investigation of emissions and LTR
176 strength are performed with the computationally cheaper, coarser horizontal resolution
177 configuration of the model (i.e. 6° in longitude by 4° in latitude).

178 *2.3 Global model evaluation methodology*

179 The model's performance has been evaluated by comparing the simulated O₃ and CO levels with
180 surface observations, ozonesonde data and satellite retrievals, all for the year 2008. O₃ surface
181 observations are taken from the European Monitoring Evaluation Program network (EMEP;
182 www.emep.int) and from the World Ozone and Ultraviolet Radiation Data Centre (WOUDC;
183 <http://www.woudc.org>) (the location of all surface observational sites used for model evaluation
184 is provided in the supplementary material Table S1 and Fig. S1). Ozonesonde data from sites
185 around the world provided by the WOUDC are used to evaluate the computed vertical structure

186 of O₃. CO surface observations around the globe for the year 2008 are taken from World Data
187 Centre for Greenhouse Gases (WDCGG; <http://ds.data.jma.go.jp/gmd/wdcgg/>).

188 TM4-ECPL results for tropospheric O₃ and CO have been further compared with data from the
189 Tropospheric Emission Spectrometer (TES) satellite instrument. TES is a high resolution (0.1
190 cm⁻¹), infrared, Fourier Transform spectrometer aboard the NASA Aura satellite that follows a
191 polar Sun - synchronous orbit with an equator crossing time at 01:45 and 13:45 local time, and
192 has a repeating cycle of 16 days. The version 4 of TES global survey data, focusing on the FT
193 region of 800-400 hPa, are used here following the methods presented by Voulgarakis et al.
194 (2011). The TES products are provided in 67 levels in the vertical with a varying layer thickness
195 and with an averaged nadir footprint of 5 km by 8 km (Beer, 2006). Model 3-hourly output is
196 sampled at the times and locations of the TES measurements. The model values are
197 logarithmically interpolated onto the 67 TES pressure levels in the vertical, and the TES a priori
198 profiles and averaging kernels are applied. The processed observational and model data are
199 regridded to a 3°x2° grid (in longitude by latitude horizontal resolution).

200 To quantify the model's ability in simulating O₃ and CO levels, statistical parameters commonly
201 used for model validation have been calculated: the correlation coefficient (R), the standard error
202 (STD), the normalized mean bias (NMB), the normalized mean error (NME) and the root mean
203 square error (RMSE). In short, R reflects the strength of the linear relationship between model
204 results and observations (the ability of the model to simulate the observed variability), and it is
205 insensitive to either an additive or a multiplicative factor; STD is a numerical value indicating
206 the reliability of the mean, estimated by the sample standard deviation divided by the square root
207 of the sample size; MNE and MNB indicate the errors and biases towards overestimations;
208 RMSE is a measure of mean relative scatter reflecting both systematic and random errors. All
209 equations used for the statistical analysis of model results are provided in the supplementary
210 material (Eq. S1-S5).

211 *2.4 Budget Calculations*

212 To calculate the pollutant budget, the atmosphere has been divided into three vertical zones; the
213 boundary layer (BL; from the surface up to 850hPa – the 6 first levels of the model), the free
214 troposphere (FT; between 850hPa and the tropopause –the next 13 levels of the model) and the
215 stratosphere (ST; from the tropopause up to the top of the model's atmosphere 0.1hPa – the top

216 15 levels of the model). Pollutant lateral fluxes through the boundaries of the studied region have
217 been calculated for these three vertical zones as well as vertical exchange fluxes between the BL
218 and the FT and between the FT and the ST. Emissions, chemical production, chemical
219 destruction and deposition have also been computed for the budget analysis. The tropopause in
220 the model is here determined by the lowest grid boxes where monthly mean O₃ concentrations
221 are greater than 150 ppb_v (i.e. the chemical tropopause as in Stevenson et al., 2006). The
222 chemical production of O₃, which occurs through the oxidation of CO, CH₄, and NMVOCs in the
223 presence of NO_x, is here computed as the sum of the change in O₃ concentration due to chemistry
224 (net chemical production) and the O₃ chemical loss computed as the sum of the reactions that
225 destroy O₃. These are O₃ photolysis followed by the reaction of the produced excited oxygen
226 atom with water vapour to form OH radical and O₃ reactions with alkenes, hydrogen peroxy and
227 hydroxyl radicals (for the reactions see Myriokefalitakis et al., 2008). All budget terms are
228 calculated every model time step and averaged/integrated appropriately. Lifetimes are calculated
229 by dividing the burden with the respective loss budget term.

230 **3. Results and discussion**

231 Evaluation of the factors that control surface O₃ and CO levels as reflected in atmospheric air
232 quality modeling is critical for air-quality strategies while an accurate simulation of vertical
233 profiles is important for O₃ climate forcing calculations. In this respect, first the simulated
234 distributions of O₃ and CO for the year 2008 are evaluated and then their budget over the
235 Mediterranean and the impact of specific sources to the surface air pollution levels are discussed.

236 *3.1 Evaluation of O₃ and CO distributions*

237 *3.1.1 Evaluation of Surface O₃*

238 To compare observations with model results, EMEP stations have been first divided into four
239 groups, representing different regions of Europe; namely: a) Northwestern Europe (45°N – 60°N;
240 10°W - 15°E), b) Northeastern Europe (45°N - 60°N; 15°E - 40°E), c) Southwestern Europe
241 (30°N - 45°N; 10°W - 15°E) and d) Southeastern Europe (30°N - 45°N; 15°E - 40°E). Monthly
242 model results are interpolated for each station's coordinates and averaged separately for each
243 group to provide monthly mean surface concentrations of all stations for each of the 4 different
244 European domains (Fig. 1). Note that the number of stations varies between regions and that for

245 each region the monthly observational data and the respective standard errors as well as model
246 calculations (for every station's coordinates) have been averaged appropriately.

247 Fig. 1a shows that for the Northwestern European domain, the model overestimates the available
248 observations in summer ($R=0.8$; $MNB=24\%$). The same pattern is simulated for the Northeastern
249 European domain (Fig. 1b; $R=0.9$; $NMB=27.2\%$) where the model also overestimates observed
250 O_3 in summer. For both, the Southeastern and the Southwestern parts of Europe (Fig. 1d and Fig.
251 1c, respectively), TM4-ECPL satisfactorily reproduces the observed variability of concentrations
252 ($R=0.8$) but with a general tendency to overestimate Southwestern Europe surface O_3 in summer
253 (up to 60 ppb_v in summer, $NMB=21.8\%$, while much smaller overestimate is found for
254 Southeastern Europe; $NMB=7.5\%$). However, the general summertime model overestimation of
255 surface O_3 compared to observations implies a potentially strong photochemical O_3 production
256 calculated by the model, especially in the Western part of the Mediterranean, where the model
257 predicts O_3 concentrations for the period from May to September that are higher than the 84.1
258 percentile ($+1\sigma$, standard deviation) of the measurements (Fig. 1c). These discrepancies can be
259 attributed to the inaccuracies in emissions of O_3 precursors and to the model's coarse resolution
260 that implies limited accuracy of non-linearities in chemistry (Kanakidou and Crutzen, 1999).
261 Another possible reason of the departure of O_3 simulated concentrations from observations
262 during summer is the simulation of the dry deposition O_3 flux.

263 Simulated surface O_3 is further evaluated on a global scale against available surface observations
264 from the WOUDC, for the year 2008. Fig. S2a presents the point-by-point (scatter plot) of all
265 available measurements from WOUDC and EMEP stations. Observed O_3 mixing ratios are
266 generally well reproduced by the model ($R=0.7$, $RSME = 11.9$ ppb_v), but the model in general
267 tends to overestimate the observations ($MNB = 15.2\%$).

268 *3.1.2 Evaluation of O_3 vertical structure*

269 Ozonesonde observations compiled by the WOUDC have also been used to evaluate the models'
270 capability in reproducing the O_3 observed vertical profiles. Fig. 2 presents the comparison of
271 model results with observations in 2008 at the Hohenpeissenberg (Germany) and Payerne
272 (Switzerland) ozonesonde stations for five pressure levels (900 hPa, 800 hPa, 500 hPa, 400 hPa
273 and 200 hPa), covering boundary layer and the low and high free troposphere. In order to
274 compare with the WOUDC observations, both the model results and the ozonesondes

275 observations have been firstly linearly interpolated into layers of 50 hPa from the surface to the
276 top of the atmosphere. Comparisons for the other European stations available by WOUDC (i.e.
277 Lindenber – Germany; Legiovo – Poland; De Bilt – The Netherlands; Ankara – Turkey) are
278 further presented in the supplementary material (Fig. S3). The model captures the O₃ distribution
279 quite well almost at all sites throughout the lower troposphere. Differences in the model
280 performance at the various stations can be due to the different characteristics of the stations, for
281 instance the O₃ precursor source regions, the intensity of photochemistry and the major transport
282 patterns that are affecting them. Above 200hPa model overestimations are mainly attributed to
283 the upper boundary conditions applied in the model (see Section 2.1). The point-by-point
284 comparison of monthly mean values for all WOUDC ozonesonde tropospheric observations sites
285 for the year 2008 (2344 pairs) is also presented in Fig. S2b. Globally, the model overestimates
286 observations by roughly 20% (R = 0.8, NMB = 10.6%, NME 20%). Similar performance is also
287 found over Europe (Fig. S2b).

288 *3.1.3 Evaluation of Free Tropospheric O₃ Concentrations*

289 Simulated O₃ concentrations are further compared to the TES satellite retrievals for the
290 middle/low FT. Fig. 3a depicts the annual mean calculated O₃ concentrations between 800 and
291 400 hPa (the vertical region with the maximum TES instrument sensitivity) over Europe
292 calculated by TM4-ECPL and Fig. 3c shows the percentage difference from TES retrievals. The
293 model tends to overestimate the mean free tropospheric O₃ concentrations retrieved from TES
294 observations over Northern Europe and Scandinavia (up to 3%), while simulated O₃
295 concentrations are underestimated up to 5% in the EM.

296 Fig. S4 also shows the seasonality in the zonal mean (60°S – 60°N) O₃ concentrations in the free
297 troposphere (800 - 400hPa) as computed by the model and its difference from the TES
298 observations. This comparison reveals an O₃ overestimate by the model (up to about 10%) in the
299 northern high latitude regions during the summer months and an underestimate in lower latitudes
300 that reaches 15% in the tropics during NH spring-summer. However, it is worth to note here that
301 the disagreement between TM4-ECPL and TES could be partially explained by the observed
302 TES positive bias between 3-10 ppbv (Nassar et al., 2008).

303 3.1.4 Evaluation of surface CO concentrations

304 TM4-ECPL results have also been compared with surface CO observations from the WDCGG
305 database for the year 2008. Fig. 4 presents the CO comparison of monthly mean model results
306 with observations for countries within Europe; although the number of the CO monitoring
307 stations is limited (8 stations for the year 2008 over Europe). For this comparison, monthly
308 model results have been extracted for each station and an average for all stations in the same
309 country has been obtained. Fig. 4 shows that the model satisfactorily simulates the CO surface
310 concentrations for Germany (R = 0.7, NMB= -4.9%), Slovenia (R = 0.6, NMB = -2.8%) and
311 Switzerland (R = 0.6, NMB = -3.3%), while an offset is found for the station in The Netherlands
312 (R = 0.9, NMB= -26.6%). The model evaluation for all CO surface observational sites over
313 Europe and the globe for the year 2008 is also presented in Fig. S2c, based on monthly mean
314 values. The point-by-point global comparison shows that the model generally underestimates the
315 observations (NMB = -21%) but captures the variability (R = 0.9).

316 3.1.5 Evaluation of Free Tropospheric CO concentrations

317 Simulated CO concentrations in the lower free troposphere are also compared with the TES
318 products. Fig. 3b depicts the annual mean CO concentrations between 800-400 hPa over Europe
319 calculated by TM4-ECPL and Fig. 3d shows the percentage difference between the model results
320 and the CO TES product for 2008. The model underestimates the annual mean CO
321 concentrations over Europe by about 10%. The seasonality of the zonal mean CO concentrations
322 between 60°S and 60°N in the middle/low free troposphere (800-400hPa) as calculated by TM4-
323 ECPL is presented in Fig. S4b. The model calculates a winter and a spring maximum in the
324 Northern Hemisphere (NH), and less than half concentrations in the Southern Hemisphere.
325 Secondary maxima due to biomass burning processes are also simulated for the tropics from
326 August to February. The model tends to underestimate CO summer concentrations in the NH. In
327 the NH subtropics (0° – 30°N) the model underestimation of CO concentrations reaches almost
328 20% from April to late June (Fig. S4d). On the contrary, the model tends to overestimate the
329 retrieved CO tropospheric concentrations by about 10% in the mid-latitudes from September to
330 December. Note however, that studies of TES CO products validation against aircraft data have
331 shown a small bias of TES products that was slightly negative (<10 %) in mid-latitudes and
332 slightly positive (<10 %) in the tropics (Luo et al., 2007; Lopez et al., 2008). Thus, some TM4-
333 ECPL disagreement (Fig. S4f) can be attributed to observational errors. The tendency to

334 underestimate northern extratropical CO and to overestimate tropical CO in the free troposphere
335 is, however, a common feature in current atmospheric modelling (e.g. Naik et al., 2013).

336 *3.2 Tropospheric budget analysis for O₃ and CO*

337 *3.2.1 Global troposphere*

338 Global tropospheric burden for O₃ and CO governed by both sources (i.e., the chemical
339 production and the stratosphere-troposphere exchanges for O₃, and emissions and chemical
340 production for CO) and sinks (chemical destruction and deposition for both O₃ and CO) have
341 been calculated for the year 2008. Large O₃ chemical production (5294 Tg yr⁻¹) and chemical
342 destruction (5031 Tg yr⁻¹) terms are calculated, while dry deposition flux (753 Tg yr⁻¹) and
343 stratospheric net influx (490 Tg yr⁻¹) are computed to be an order of magnitude lower. These
344 values are well in the range of the 26 model results that participated in the Stevenson et al.
345 (2006) model intercomparison study for the year 2000 (chemical production of 5110 ± 606 Tg
346 yr⁻¹, a chemical destruction of 4668 ± 727 Tg yr⁻¹, a dry deposition flux of 1003 ± 200 Tg yr⁻¹
347 and a stratospheric influx of 552 ± 200 Tg yr⁻¹). Similarly, the mean tropospheric O₃ burden of
348 345 Tg here calculated is close to the 344 ± 39 Tg O₃ tropospheric burden derived by Stevenson
349 et al. (2006).

350 For the year 2008 in the TM4-ECPL, global CO primary emissions amount 896 Tg yr⁻¹, global
351 CO chemical production is calculated to be 1946 Tg yr⁻¹ that is about twice the primary
352 emissions and chemical destruction to be 2647 Tg yr⁻¹. The total CO source (i.e. emissions and
353 chemical production, 2427 Tg yr⁻¹ for 2008) is in agreement with earlier studies; e.g. about 2760
354 Tg yr⁻¹ for the year 1997 derived by Müller and Stavrou (2005) using inverse modeling
355 calculated the global CO source and 2455 Tg yr⁻¹ calculated by Kanakidou and Crutzen (1999).
356 The chemical destruction of CO in the model is due to the oxidation by OH radicals. OH radical
357 oxidation is also the primary loss mechanism for methane (CH₄) and for this OH atmospheric
358 burden is commonly studied simultaneously to CH₄ chemical lifetime. For the year 2008, the
359 TM4-ECPL calculates a tropospheric chemical lifetime of CH₄ of about 8.1 years, which is close
360 to the low-end of mean tropospheric chemical CH₄ lifetime due to OH oxidation for the year
361 2000, as derived from the ACCMIP (Atmospheric Chemistry and Climate Modeling
362 Intercomparison Project) multi-model mean (9.8 ± 1.6 yr; Voulgarakis et al., 2013). CO
363 tropospheric burden calculated by TM4-ECPL is 317 Tg for the year 2008, similar to the

364 estimate by Kanakidou and Crutzen (1999) and by 20% lower than the 397 Tg calculated by
365 Müller and Stavrou (2005). However, the dry deposition sink calculated both by Bergamaschi
366 et al. (2000) (288 Tg yr⁻¹) and by Müller and Stavrou (2005) (186-205 Tg yr⁻¹) is larger than
367 the deposition flux of about 172 Tg yr⁻¹ calculated by TM4-ECPL.

368 3.2.2 Eastern Mediterranean

369 Fig. 5 and Fig. 6 sketch the budget calculations over the Mediterranean, for O₃ and for CO
370 respectively, separating also the Western from the Eastern basin (shaded/non - shaded areas) and
371 the BL (lower parts) from the FT (upper parts). For the BASE simulation, in the EM-BL O₃ is
372 imported from the North (5 Tg yr⁻¹), from the western boundary (20 Tg yr⁻¹) and from the EM-
373 FT aloft (36 Tg yr⁻¹) and exported mainly to the South (38 Tg yr⁻¹) and to the East (24 Tg yr⁻¹).
374 This result further indicates the significance of free tropospheric O₃ intrusions for the EM O₃
375 abundance in the BL. Photochemistry in the EM-BL (involving NO_x, VOCs photo-oxidation)
376 acts as an additional significant source for O₃ in the region with a net chemical production
377 calculated to about 12 Tg yr⁻¹. For CO, the model calculates for the EM-BL a burden of 0.6 Tg of
378 CO, a chemical production of 10 Tg yr⁻¹, primary emissions in the region of 8 Tg yr⁻¹ and a dry
379 deposition flux of 3 Tg yr⁻¹. Free-tropospheric intrusion imports 22 Tg yr⁻¹ of CO to the EM-BL
380 and 20 Tg yr⁻¹ of CO are advected from the west. The model also calculates a strong CO outflow
381 of 32 Tg yr⁻¹ to the South and a weaker import from the northern boundary that accounts about 6
382 Tg yr⁻¹.

383 As far as it concerns the EM-FT (Fig. 5 and Fig. 6; upper parts), significant amounts of O₃ and
384 CO are advected through the western boundary (383 Tg yr⁻¹ and 228 Tg yr⁻¹, respectively) and
385 even larger amounts are exported due to chemical build-up and LRT to the East (445 Tg yr⁻¹ and
386 240 Tg yr⁻¹, respectively). Three times higher O₃ burden over the EM (2.1 Tg) is simulated in the
387 FT than the BL, while O₃ residence time over the EM is calculated to be about 2.7 days in the BL
388 and about 1.5 days in the FT. The model simulates a net O₃ photochemical source of 3 Tg yr⁻¹
389 and a CO net chemical destruction of about 4 Tg yr⁻¹ in the EM-FT. Subsidence from higher
390 atmospheric layers is an important source for both O₃ (48 Tg yr⁻¹) and CO (12 Tg yr⁻¹) in the
391 EM-FT. Moreover, northern winds enriched in O₃ and CO carry significant amounts of these
392 pollutants to the region's FT (39 Tg yr⁻¹ and 25 Tg yr⁻¹, respectively), while about 17 Tg yr⁻¹ of
393 O₃ are also imported from the southern boundary to the EM-FT, partly resulting from transport
394 from Asia and Africa (17% and 16% respectively).

395 3.2.3 *Western Mediterranean and comparison to the Eastern basin*

396 Fig. 5 and Fig. 6 (shaded area) also depict O₃ and CO budgets in the Western Mediterranean
397 (WM). TM4-ECPL calculates a significant influence from the surroundings since advection of
398 pollutants into the WM-FT (sum of all import terms) is about 2 orders of magnitude higher than
399 the net photochemical source in this region.

400 The WM-BL is receiving 4 times lower amounts of O₃ from the FT (9 Tg yr⁻¹) than the Eastern
401 basin, and the chemical production of O₃ (36 Tg yr⁻¹) is slightly lower than that for EM.
402 According to TM4-ECPL model calculations, stratospheric O₃ intrusions are an important source
403 (75 Tg yr⁻¹) of tropospheric O₃ over the entire Mediterranean. However, over the WM smaller O₃
404 amounts are computed (roughly 36% of the total stratospheric intrusions), due to the stagnant
405 conditions in the BL (Millán et al., 2005) as compared to the EM, even though an O₃ burden of
406 about 2.1 Tg in the WM-FT is also calculated as for the case of EM-FT. In the WM-BL, the O₃
407 chemical lifetime is calculated to be about 12.7 days while the overall residence time in the
408 western basin is estimated at about 4.7 days (i.e. about 33% longer than that in the EM) due to
409 deposition and fast outflow. Ventilation by advection is about 3 times faster in the EM than in
410 the WM (about 4 days versus 12 days, respectively). However, the chemical lifetime of O₃ in the
411 BL is almost identical in the two basins (about 12 days) while the subsidence from the FT is
412 about 4 times higher in the EM than in the WM. Overall, the EM-BL is acting as a receptor of O₃
413 of air masses mainly from the FT (59%) and the WM (33%), as well as a source of O₃ and CO
414 for the downwind locations to the South (60%) and the East (40%). Air-masses advected from
415 the North are about 2 times richer in O₃ in the WM-FT than in the EM-FT, even though the
416 subsidence from the stratosphere provides about 78% more O₃ in the EM-FT than in the WM-
417 FT.

418 3.3 *Contribution of sources to air pollution*

419 TM4-ECPL calculations show that the Mediterranean (Fig. 7c) is among the regions
420 experiencing the highest surface O₃ concentrations in the globe together with eastern U.S. and
421 Central Asia (Fig. 7a). In general, TM4-ECPL calculates high surface O₃ concentrations in the
422 mid-latitudes of the NH, over regions with high anthropogenic activity (US, Europe and China)
423 as well as in the tropical areas affected by biomass burning emissions (Fig. 7a). The zonal mean
424 distribution of O₃ concentrations (not shown) presents enhanced values in the sub-tropics

425 because of O₃ production in regions affected by biomass burning such as Central Africa. The
426 model also calculates high O₃ concentrations in the pollution plumes over the Atlantic and the
427 outflow over Japan.

428 Simulated surface CO also shows enhanced concentrations over polluted regions of the NH (i.e.
429 US, Europe and China) as well as the biomass burning peaks over Central Africa and the
430 Amazon Basin (Fig. 7b). Although, primary CO sources are mainly from anthropogenic origin
431 (roughly 60%), CO secondary sources from VOC oxidation are calculated to be by 70% from
432 CH₄ and by 30% from NMVOCs (e.g. Poisson et al., 2000). The CO zonal mean distribution (not
433 shown) clearly shows the high NH concentrations, resulting from both high primary and
434 secondary sources north of 30°S. TM4-ECPL calculates higher CO concentrations in the winter
435 (not shown) mainly due to the lower loss by reaction with OH that presents a seasonal wintertime
436 minimum in the troposphere (reduced oxidizing capacity).

437 In order to investigate the contribution of local and distant sources to air pollution in the BL,
438 emission perturbation simulations have been performed and compared to the base case
439 simulation (BASE) as previously explained in Section 2.2. Percent differences were calculated as
440 $100 \cdot (\text{BASE} - \text{MaskX}) / \text{BASE}$; where MaskX is the respective sensitivity simulation as presented
441 in Table 1.

442 *3.3.1 O₃ surface concentrations*

443 The model (BASE) calculates a surface annual O₃ mean mixing ratio of about 43 ppb_v over the
444 European domain in the model (Fig. 7c), with a maximum exceeding 55 ppb_v over the central
445 and Eastern Mediterranean. The calculations attribute up to 15% of the O₃ surface concentrations
446 to the regional anthropogenic emissions in the EM (MaskAnthro vs. BASE), with an annual
447 mean contribution in the EM of about 8% (Fig. 8a). Additionally, up to 5% on an annual basis is
448 associated with biogenic emissions (MaskBIO vs. BASE), but less than 1% is due to biomass
449 burning emissions (MaskBB vs. BASE). All regional emissions accounted by the model
450 (MaskALL vs. BASE) are responsible for about 11% of O₃ surface levels on annual base, with a
451 maximum contribution of 18% over and south of the Levantine Sea (Fig. 8c), indicating thus the
452 importance of air-mass transport from neighboring regions (i.e. LRT by advection and
453 subsidence to the region). When European emissions are neglected (MaskeU vs. BASE), the
454 model calculates about 13% of reduction in O₃ surface concentrations over the EM (Fig. S5a).

455 Northern America's emissions (Fig. S5b) affect the surface O₃ concentrations over the entire
456 European continent by about 5% (MaskNAM vs. BASE). Asian emissions (MaskAS vs. BASE)
457 affect O₃ surface concentrations by 10% on annual basis (Fig. S5c), while the African continent's
458 emissions (MaskAF vs. BASE) contribute about 4% to EM basin surface O₃ concentrations (Fig.
459 S5d).

460 3.3.2 CO surface concentrations

461 For CO concentrations over Europe, the model calculates a surface annual mean mixing ratio of
462 110 ppb_v, with a maximum concentration of 128 ppb_v over EM (Fig. 7d). Anthropogenic local
463 emissions in the EM contribute by 18% to the surface CO levels in the EM (Fig. 8b) annually.
464 Maximum anthropogenic contribution (roughly 32%) to surface CO concentrations is calculated
465 over Cairo. On the other hand, CO concentrations over the EM are associated by about 9% on
466 annual basis with regional biogenic VOC oxidation (not shown) and about 3% are due to
467 biomass burning emissions (not shown). All regional emissions accounted by the model (Fig. 8d)
468 are responsible for 23% of CO surface levels, while the remaining could be attributed to LRT.
469 On an annual basis, European emissions (MaskEU) contribute by about 25% to the calculated
470 CO surface concentrations over the EM (Fig. S6a), Northern America's emissions (MaskNAM)
471 by 12% (Fig. S6b), Asian emissions (MaskAS) by 26% (Fig. S6c) and African emissions
472 (MaskAF) by 11% (Fig. S6d).

473 3.4 Projected changes due to anthropogenic emissions

474 In Fig. 8e and 8f, the simulation using anthropogenic emissions as projected for the year 2050
475 (FUTURE) is compared to the BASE (i.e. $100 \times (\text{FUTURE} - \text{BASE}) / \text{BASE}$). A 16% increase in
476 surface O₃ over central Europe is due to the reduction in NO_x anthropogenic emissions (a
477 reduction in the NO_x O₃-titration effect), while a decrease in surface O₃ by about 11% is
478 calculated for the Mediterranean (Fig. 8e) is due to the reduction in O₃ chemical formation and to
479 import/export fluxes changes. On the opposite, CO surface concentrations are calculated to
480 decrease by about 10% over central Europe. This change is the overall effect of the decrease
481 (more than 40%) in the primary anthropogenic emissions, an almost similar in magnitude
482 increase in the OH radical concentrations (affecting both the secondary CO source and the
483 chemical sink of CO) and changes in the transport fluxes. The opposite trend is projected for the
484 EM, where an increase (Fig. 8f) by about 10% in CO surface concentrations is computed. This

485 change reflects mainly the increase of CO primary anthropogenic emissions in the south
486 combined with a reduction in surface OH levels by about 20% (e.g. due to smaller precursor O₃
487 concentrations) that leads to a reduction in both the secondary source and in the chemical sink of
488 CO in the EM.

489 All FUTURE O₃ imports compared to the BASE simulation (computed as $[100 \times (\text{FUTURE} - \text{BASE}) / \text{BASE}]$) due to advection to EM-BL are calculated to decrease roughly by 13% on
490 average, with the Northern boundaries imports to decrease, however, by about 17%. On the other
491 hand, exports from the EM-BL are also calculated to decrease under 2050 anthropogenic
492 emissions, mainly to the South (14%). Note that the same decrease is also calculated for the EM-
493 FT, resulting thus to a decrease in downdraft to EM-BL of about 13%. As far as it concerns the
494 CO, in the EM-BL increases in CO imports from the EM-FT boundary and from the West (about
495 24% and 17%, respectively) are calculated. In contrast, a decrease in import from the North of
496 about 14% is also calculated for EM-BL, which can also be attributed to impact of Asian
497 emissions as discussed in the previous section (Section 3.3.2). CO has a longer lifetime
498 compared to O₃, which makes the LRT Asian contribution to European pollution more
499 pronounced on CO than on O₃ within Europe (i.e. Fig. S6c). For the FUTURE simulation, both
500 meteorology and CH₄ concentrations are kept constant in the model, thus the increase in CO
501 chemical production and destruction is attributed to the respective increase in O₃ levels and thus
502 in OH production, leading to a more aggressive CO loss. As explained in section 2.1 changes in
503 meteorology and the stratospheric boundary conditions, which may occur in the future under
504 climate change, are not taken into account by the model. Thus, the computed anti-correlation
505 between O₃ and CO future changes over the EM is driven by the changes in anthropogenic
506 emissions and the induced differences in the oxidation capacity.

508 **4. Conclusions**

509 The global chemistry-transport model TM4-ECPL is able to reproduce observations of O₃ and
510 CO at the surface, the BL and in FT in the rural and remote atmosphere over Europe. This
511 allowed us to analyze the O₃ and CO budget over the EM. We found that the EM atmosphere is
512 strongly affected by air masses from surrounding regions and thus by sources other than local.
513 Similar conclusions for the EM, documented in different ways, have been reached by other
514 modeling studies (e.g. Im and Kanakidou, 2012; Zanis et al., 2014) as well as in the reviews by
515 Kanakidou et al. (2011) and Kallos et al. (2013) and references therein. In the present study we

516 further quantified the contribution of various sources to the O₃ and CO budget in the EM. In
517 particular, our calculations show that local anthropogenic emissions are responsible for about 8%
518 of surface O₃ concentration and 18% of CO surface concentrations, while downward transport
519 from the FT provides about 38% of O₃ sources and about 33% of CO sources into the EM-BL
520 and horizontal advection from the surrounding regions contributes by about 51% and 27%,
521 respectively. Therefore, neglecting all the emissions in the EM region (i.e. anthropogenic,
522 biomass burning, biogenic and natural emissions) leads to a reduction in annual mean surface
523 concentrations of only 11% in O₃ and of 23% in CO.

524 For anthropogenic emissions projected for the year 2050, the model calculates a reduction of
525 about 11% in the regional O₃ surface concentrations, with a contemporaneous increase in CO
526 surface concentrations of roughly 10% in the EM. The opposite changes of O₃ and CO due to
527 future anthropogenic emissions could be attributed to the respective changes of oxidation
528 capacity within the EM and to changes in the fluxes in and out the EM which are driven by
529 large-scale concentration changes. However, our calculations do not account for potential
530 changes in meteorology and stratospheric boundary conditions. Overall, this work indicates that
531 O₃ and CO surface levels in the EM are mainly driven by LRT of pollution and related
532 precursors within the BL, but also through the FT and subsequent downdraft to the BL. This
533 implies that mitigation of local anthropogenic emissions is not sufficient for significant
534 improvements in air quality in the Mediterranean region, and that coordinated efforts between
535 the countries surrounding and located upwind of the basin are required.

536

537 **Acknowledgements**

538 This work has been initiated in the frame of the CityZEN project (megaCITY - Zoom for the
539 Environment, FP7-ENV-2008-212095) and has been finalized with support to SM and GSF by
540 ECLIPSE (Evaluating the CLimate and Air Quality ImPacts of Short-livEd Pollutants, FP7-
541 ENV-2011-282688) and to ND by PEGASOS (Pan - European Gas - AeroSOls - climate
542 interaction Study, FP7-ENV-2010-265148) collaborative projects funded by the European
543 Commission. We thank Prof. N. Mihalopoulos and Dr. G. Kouvarakis for Finokalia station data
544 availability and the World Ozone and Ultraviolet Radiation Data Centre (WOUDC) for
545 ozonesondes data availability.

546

547 **References**

- 548 Ainsworth, E.A., Yendrek, C.R., Sitch, S., Collins, W.J., Emberson, L.D., 2012. The effects of
549 tropospheric ozone on net primary productivity and implications for climate change. *Annu.*
550 *Rev. Plant Biol.* 63, 637–61. doi:10.1146/annurev-arplant-042110-103829
- 551 Beekmann, M., Vautard, R., 2010. A modelling study of photochemical regimes over Europe:
552 Robustness and variability. *Atmos. Chem. Phys.* 10, 10067–10084. doi:10.5194/acp-10-
553 10067-2010
- 554 Beer, R., 2006. TES on the aura mission: scientific objectives, measurements, and analysis
555 overview. *IEEE Trans. Geosci. Remote Sens.* 44, 1102–1105.
556 doi:10.1109/TGRS.2005.863716
- 557 Bergamaschi, P., Hein, R., Heimann, M., Crutzen, P.J., 2000. Inverse modeling of the global CO
558 cycle: 1. Inversion of CO mixing ratios. *J. Geophys. Res.* 105, 1909.
559 doi:10.1029/1999jd900818
- 560 Brohede, S., McLinden, C.A., Urban, J., Haley, C.S., Jonsson, A.I., Murtagh, D., 2008. Odin
561 stratospheric proxy NO_y measurements and climatology. *Atmos. Chem. Phys.* 8, 5731–
562 5754. doi:10.5194/acp-8-5731-2008
- 563 Colette, A., Granier, C., Hodnebrog, Ø., Jakobs, H., Maurizi, A., Nyiri, A., Rao, S., Amann, M.,
564 Bessagnet, B., D'Angiola, A., Gauss, M., Heyes, C., Klimont, Z., Meleux, F.,
565 Memmesheimer, M., Mieville, A., Rouil, L., Russo, F., Schucht, S., Simpson, D., Stordal,
566 F., Tampieri, F., Vrac, M., 2012. Future air quality in Europe: a multi-model assessment of
567 projected exposure to ozone. *Atmos. Chem. Phys.* 12, 10613–10630. doi:10.5194/acp-12-
568 10613-2012
- 569 Crutzen, P.J., 1974. Photochemical reactions initiated by and influencing ozone in unpolluted
570 tropospheric air. *Tellus* 26, 47–57. doi:10.1111/j.2153-3490.1974.tb01951.x
- 571 Daskalakis, N., Myriokefalitakis, S., Kanakidou, M., 2015. Sensitivity of tropospheric loads and
572 lifetimes of short lived. *Atmos. Chem. Phys.* 15, 3543–3563. doi:10.5194/acp-15-3543-
573 2015
- 574 Dee, D.P., Uppala, S.M., Simmons, A.J., Berrisford, P., Poli, P., Kobayashi, S., Andrae, U.,
575 Balsameda, M.A., Balsamo, G., Bauer, P., Bechtold, P., Beljaars, A.C.M., van de Berg, L.,
576 Bidlot, J., Bormann, N., Delsol, C., Dragani, R., Fuentes, M., Geer, A.J., Haimberger, L.,
577 Healy, S.B., Hersbach, H., Hólm, E. V, Isaksen, L., Kållberg, P., Köhler, M., Matricardi,
578 M., McNally, A.P., Monge-Sanz, B.M., Morcrette, J.J., Park, B.K., Peubey, C., de Rosnay,
579 P., Tavolato, C., Thépaut, J.N., Vitart, F., 2011. The ERA-Interim reanalysis: configuration
580 and performance of the data assimilation system. *Q. J. Roy. Meteor. Soc.* 137, 553–597.
581 doi:10.1002/qj.828
- 582 Derwent, R.G., Jenkin, M.E., Saunders, S.M., 1996. Photochemical ozone creation potentials for
583 a large number of reactive hydrocarbons under European conditions. *Atmos. Environ.* 30,
584 181–199. doi:10.1016/1352-2310(95)00303-G
- 585 Drori, R., Dayan, U., Edwards, D.P., Emmons, L.K., Erlick, C., 2012. Attributing and
586 quantifying carbon monoxide sources affecting the Eastern Mediterranean: a combined
587 satellite, modelling, and synoptic analysis study. *Atmos. Chem. Phys.* 12, 1067–1082.
588 doi:10.5194/acp-12-1067-2012
- 589 Eckhardt, S., Quennehen, B., Olivie, D.J.L., Berntsen, T.K., Cherian, R., Christensen, J.H.,

- 590 Collins, W., Crepinsek, S., Daskalakis, N., Flanner, M., Herber, A., Heyes, C., Hodnebrog,
591 Ø., Huang, L., Kanakidou, M., Klimont, Z., Langner, J., Law, K.S., Lund, M.T., Mahmood,
592 R., Massling, A., Myriokefalitakis, S., Nielsen, I.E., Nøjgaard, J.K., Quaas, J., Quinn, P.K.,
593 Raut, J.-C., Rumbold, S.T., Schulz, M., Sharma, S., Skeie, R.B., Skov, H., Uttal, T., Salzen,
594 K. von, Stohl, A., 2015. Current model capabilities for simulating black carbon and sulfate
595 concentrations in the Arctic atmosphere: a multi-model evaluation using a comprehensive
596 measurement data set. *Atmos. Chem. Phys.* 15, 9413–9433. doi:doi:10.5194/acp-15-9413-
597 2015
- 598 Fountoukis, C., Nenes, A., 2007. ISORROPIA II: a computationally efficient thermodynamic
599 equilibrium model for K^+ - Ca^{2+} - Mg^{2+} - NH_4^+ - Na^+ - SO_4^{2-} - NO_3^- - Cl^- - H_2O aerosols.
600 *Atmos. Chem. Phys.* 7, 4639–4659. doi:10.5194/acp-7-4639-2007
- 601 Gerasopoulos, E., Amiridis, V., Kazadzis, S., Kokkalis, P., Eleftheratos, K., Andreae, M.O.,
602 Andreae, T.W., El-Askary, H., Zerefos, C.S., 2011. Three-year ground based measurements
603 of aerosol optical depth over the Eastern Mediterranean: the urban environment of Athens.
604 *Atmos. Chem. Phys.* 11, 2145–2159. doi:10.5194/acp-11-2145-2011
- 605 Gerasopoulos, E., Kouvarakis, G., Vrekoussis, M., Kanakidou, M., Mihalopoulos, N., 2005.
606 Ozone variability in the marine boundary layer of the eastern Mediterranean based on 7-
607 year observations. *J. Geophys. Res. D Atmos.* 110, 1–12. doi:10.1029/2005JD005991
- 608 Grooß, J.U., Russell III, J.M., 2005. Technical note: A stratospheric climatology for O_3 , H_2O ,
609 CH_4 , NO_x , HCl and HF derived from HALOE measurements. *Atmos. Chem. Phys.* 5,
610 2797–2807. doi:10.5194/acp-5-2797-2005
- 611 HTAP, T., 2011. Hemispheric Transport of Air Pollution 2010 Part A: Ozone And Particulate
612 Matter. *Air Pollut. Stud.*
- 613 Im, U., Kanakidou, M., 2012. Impacts of East Mediterranean megacity emissions on air quality.
614 *Atmos. Chem. Phys.* 12, 6335–6355. doi:10.5194/acp-12-6335-2012
- 615 Im, U., Markakis, K., Poupkou, A., Melas, D., Unal, A., Gerasopoulos, E., Daskalakis, N.,
616 Kindap, T., Kanakidou, M., 2011. The impact of temperature changes on summer time
617 ozone and its precursors in the Eastern Mediterranean. *Atmos. Chem. Phys.* 11, 3847–3864.
618 doi:10.5194/acp-11-3847-2011
- 619 Jimoda, L., 2012. Effects of particulate matter on human health, the ecosystem, climate and
620 materials: A review. *Facta Univ. Work. Living ...* 9, 27–44.
- 621 Kallos, G., Astitha, M., Katsafados, P., Spyrou, C., 2007. Long-Range Transport of
622 Anthropogenically and Naturally Produced Particulate Matter in the Mediterranean and
623 North Atlantic: Current State of Knowledge. *J. Appl. Meteorol. Climatol.* 46, 1230–1251.
624 doi:10.1175/JAM2530.1
- 625 Kallos, G., Mitsakou, C., Alastuey, A., van Aardenne, J., Astitha, M., Cusack, M., Doering, U.,
626 Gerasopoulos, E., Hatzianastassiou, N., Kanakidou, M., Kushta, J., Lelieveld, J., Levin, Z.,
627 Mihalopoulos, N., Millán, M., Palau, J.L., Perez, N., Pey, J., Querol, X., Solomos, S.,
628 Spyrou, C., Theodosi, C., Zerefos, C., 2013. Mechanisms of Climate Variability, Air
629 Quality and Impacts of Atmospheric Constituents in the Mediterranean Region, in: Navarra,
630 A., Tubiana, L. (Eds.), *Advances in Global Change Research*. Springer Netherlands,
631 Dordrecht, pp. 119–156. doi:10.1007/978-94-007-5781-3_4
- 632 Kanakidou, M., Crutzen, P.J., 1999. The photochemical source of carbon monoxide: Importance,

- 633 uncertainties and feedbacks. *Chemosph. - Glob. Chang. Sci.* 1, 91–109.
634 doi:[http://dx.doi.org/10.1016/S1465-9972\(99\)00022-7](http://dx.doi.org/10.1016/S1465-9972(99)00022-7)
- 635 Kanakidou, M., Mihalopoulos, N., Kindap, T., Im, U., Vrekoussis, M., Gerasopoulos, E.,
636 Dermitzaki, E., Unal, A., Koçak, M., Markakis, K., Melas, D., Kouvarakis, G., Youssef,
637 A.F., Richter, A., Hatzianastassiou, N., Hilboll, A., Ebojie, F., Wittrock, F., von Savigny,
638 C., Burrows, J.P., Ladstaetter-Weissenmayer, A., Moubasher, H., 2011. Megacities as hot
639 spots of air pollution in the East Mediterranean. *Atmos. Environ.* 45, 1223–1235.
640 doi:[10.1016/j.atmosenv.2010.11.048](https://doi.org/10.1016/j.atmosenv.2010.11.048)
- 641 Kanakidou, M., Singh, H.B., Valentin, K.M., Crutzen, P.J., 1991. A two-dimensional study of
642 ethane and propane oxidation in the troposphere. *J. Geophys. Res.* 96, 15395–15413.
643 doi:[10.1029/91jd01345](https://doi.org/10.1029/91jd01345)
- 644 Langner, J., Engardt, M., Baklanov, A., Christensen, J.H., Gauss, M., Geels, C., Hedegaard,
645 G.B., Nuterman, R., Simpson, D., Soares, J., Sofiev, M., Wind, P., Zakey, A., 2012. A
646 multi-model study of impacts of climate change on surface ozone in Europe. *Atmos. Chem.*
647 *Phys.* 12, 10423–10440. doi:[10.5194/acp-12-10423-2012](https://doi.org/10.5194/acp-12-10423-2012)
- 648 Lelieveld, J., Berresheim, H., Borrmann, S., Crutzen, P.J., Dentener, F.J., Fischer, H., Feichter,
649 J., Flatau, P.J., Heland, J., Holzinger, R., Korrman, R., Lawrence, M.G., Levin, Z.,
650 Markowicz, K.M., Mihalopoulos, N., Minikin, A., Ramanathan, V., De Reus, M., Roelofs,
651 G.J., Scheeren, H. a, Sciare, J., Schlager, H., Schultz, M., Siegmund, P., Steil, B.,
652 Stephanou, E.G., Stier, P., Traub, M., Warneke, C., Williams, J., Ziereis, H., 2002. Global
653 air pollution crossroads over the Mediterranean. *Science* 298, 794–9.
654 doi:[10.1126/science.1075457](https://doi.org/10.1126/science.1075457)
- 655 Lelieveld, J., Dentener, F.J., 2000. What controls tropospheric ozone? *J. Geophys. Res.* 105,
656 3531. doi:[10.1029/1999JD901011](https://doi.org/10.1029/1999JD901011)
- 657 Liakakou, E., Bonsang, B., Williams, J., Kalivitis, N., Kanakidou, M., Mihalopoulos, N., 2009.
658 C2–C8 NMHCs over the Eastern Mediterranean: Seasonal variation and impact on regional
659 oxidation chemistry. *Atmos. Environ.* 43, 5611–5621. doi:[10.1016/j.atmosenv.2009.07.067](https://doi.org/10.1016/j.atmosenv.2009.07.067)
- 660 Lopez, J.P., Luo, M., Christensen, L.E., Loewenstein, M., Jost, H., Webster, C.R., Osterman, G.,
661 2008. TES carbon monoxide validation during two AVE campaigns using the Argus and
662 ALIAS instruments on NASA's WB-57F. *J. Geophys. Res.* 113, D16S47.
663 doi:[10.1029/2007JD008811](https://doi.org/10.1029/2007JD008811)
- 664 Louis, J.-F., 1979. A parametric model of vertical eddy fluxes in the atmosphere. *Boundary-*
665 *Layer Meteorol.* 17, 187–202. doi:[10.1007/BF00117978](https://doi.org/10.1007/BF00117978)
- 666 Luo, M., Rinsland, C., Fisher, B., Sachse, G., Diskin, G., Logan, J., Worden, H., Kulawik, S.,
667 Osterman, G., Eldering, A., Herman, R., Shephard, M., 2007. TES carbon monoxide
668 validation with DACOM aircraft measurements during INTEX-B 2006. *J. Geophys. Res.*
669 112, D24S48. doi:[10.1029/2007JD008803](https://doi.org/10.1029/2007JD008803)
- 670 Millán, M., Estrela, M., Sanz, M., 2005. Climatic feedbacks and desertification: the
671 Mediterranean model. *J. ...* 684–701.
- 672 Molina, L.T., Molina, M.J. (Eds.), 2002. *Air Quality in the Mexico Megacity*, Alliance for
673 *Global Sustainability Bookseries*. Springer Netherlands, Dordrecht. doi:[10.1007/978-94-](https://doi.org/10.1007/978-94-010-0454-1)
674 [010-0454-1](https://doi.org/10.1007/978-94-010-0454-1)
- 675 Monks, P.S., Granier, C., Fuzzi, S., Stohl, A., Williams, M.L., Akimoto, H., Amann, M.,

- 676 Baklanov, A., Baltensperger, U., Bey, I., Blake, N., Blake, R.S., Carslaw, K., Cooper, O.R.,
677 Dentener, F., Fowler, D., Fragkou, E., Frost, G.J., Generoso, S., Ginoux, P., Grewe, V.,
678 Guenther, A., Hansson, H.C., Henne, S., Hjorth, J., Hofzumahaus, A., Huntrieser, H.,
679 Isaksen, I.S.A., Jenkin, M.E., Kaiser, J., Kanakidou, M., Klimont, Z., Kulmala, M., Laj, P.,
680 Lawrence, M.G., Lee, J.D., Liousse, C., Maione, M., McFiggans, G., Metzger, A., Mieville,
681 A., Moussiopoulos, N., Orlando, J.J., O'Dowd, C.D., Palmer, P.I., Parrish, D.D., Petzold,
682 A., Platt, U., Pöschl, U., Prévôt, A.S.H., Reeves, C.E., Reimann, S., Rudich, Y., Sellegri,
683 K., Steinbrecher, R., Simpson, D., ten Brink, H., Theloke, J., van der Werf, G.R., Vautard,
684 R., Vestreng, V., Vlachokostas, C., von Glasow, R., 2009. Atmospheric composition change
685 – global and regional air quality. *Atmos. Environ.* 43, 5268–5350.
686 doi:10.1016/j.atmosenv.2009.08.021
- 687 Müller, J.-F., Stavrou, T., 2005. Inversion of CO and NO_x emissions using the adjoint of the
688 IMAGES model. *Atmos. Chem. Phys.* 5, 1157–1186. doi:10.5194/acp-5-1157-2005
- 689 Myriokefalitakis, S., Daskalakis, N., Mihalopoulos, N., Baker, A.R., Nenes, A., Kanakidou, M.,
690 2015. Changes in dissolved iron deposition to the oceans driven by human activity: a 3-D
691 global modelling study. *Biogeosciences* 12, 3973–3992. doi:10.5194/bg-12-3973-2015
- 692 Myriokefalitakis, S., Tsigaridis, K., Mihalopoulos, N., Sciare, J., Nenes, A., Kawamura, K.,
693 Segers, A., Kanakidou, M., 2011. In-cloud oxalate formation in the global troposphere: a 3-
694 D modeling study. *Atmos. Chem. Phys.* 11, 5761–5782. doi:10.5194/acp-11-5761-2011
- 695 Myriokefalitakis, S., Vignati, E., Tsigaridis, K., Papadimas, C., Sciare, J., Mihalopoulos, N.,
696 Facchini, M.C., Rinaldi, M., Dentener, F.J., Ceburnis, D., Hatzianastasiou, N., O'Dowd,
697 C.D., van Weele, M., Kanakidou, M., 2010. Global Modeling of the Oceanic Source of
698 Organic Aerosols. *Adv. Meteorol.* 2010, 1–16. doi:10.1155/2010/939171
- 699 Myriokefalitakis, S., Vrekoussis, M., Tsigaridis, K., Wittrock, F., Richter, A., Brühl, C.,
700 Volkamer, R., Burrows, J.P., Kanakidou, M., 2008. The influence of natural and
701 anthropogenic secondary sources on the glyoxal global distribution. *Atmos. Chem. Phys.*
702 *Discuss.* 8, 1673–1708. doi:10.5194/acpd-8-1673-2008
- 703 Naik, V., Voulgarakis, A., Fiore, A.M., Horowitz, L.W., Lamarque, J.-F., Lin, M., Prather, M.J.,
704 Young, P.J., Bergmann, D., Cameron-Smith, P.J., Cionni, I., Collins, W.J., Dalsøren, S.B.,
705 Doherty, R., Eyring, V., Faluvegi, G., Folberth, G.A., Josse, B., Lee, Y.H., MacKenzie,
706 I.A., Nagashima, T., van Noije, T.P.C., Plummer, D.A., Righi, M., Rumbold, S.T., Skeie,
707 R., Shindell, D.T., Stevenson, D.S., Strode, S., Sudo, K., Szopa, S., Zeng, G., 2013.
708 Preindustrial to present-day changes in tropospheric hydroxyl radical and methane lifetime
709 from the Atmospheric Chemistry and Climate Model Intercomparison Project (ACCMIP).
710 *Atmos. Chem. Phys.* 13, 5277–5298. doi:10.5194/acp-13-5277-2013
- 711 Nassar, R., Logan, J.A., Worden, H.M., Megretskaia, I.A., Bowman, K.W., Osterman, G.B.,
712 Thompson, A.M., Tarasick, D.W., Austin, S., Claude, H., Dubey, M.K., Hocking, W.K.,
713 Johnson, B.J., Joseph, E., Merrill, J., Morris, G.A., Newchurch, M., Oltmans, S.J., Posny,
714 F., Schmidlin, F.J., Vömel, H., Whiteman, D.N., Witte, J.C., 2008. Validation of
715 Tropospheric Emission Spectrometer (TES) nadir ozone profiles using ozonesonde
716 measurements. *J. Geophys. Res.* 113, D15S17. doi:10.1029/2007JD008819
- 717 Olivieri, D.J.L., 2004. Comparison between archived and off-line diagnosed convective mass
718 fluxes in the chemistry transport model TM3. *J. Geophys. Res.* 109, D11303.
719 doi:10.1029/2003JD004036

- 720 Parrish, D.D., Singh, H.B., Molina, L., Madronich, S., 2011. Air quality progress in North
721 American megacities: A review. *Atmos. Environ.* 45, 7015–7025.
722 doi:10.1016/j.atmosenv.2011.09.039
- 723 Pausata, F.S.R., Pozzoli, L., Vignati, E., Dentener, F.J., 2012. North Atlantic Oscillation and
724 tropospheric ozone variability in Europe: model analysis and measurements
725 intercomparison. *Atmos. Chem. Phys.* 12, 6357–6376. doi:10.5194/acp-12-6357-2012
- 726 Poisson, N., Kanakidou, M., Crutzen, P., 2000. Impact of Non-Methane Hydrocarbons on
727 Tropospheric Chemistry and the Oxidizing Power of the Global Troposphere: 3-
728 Dimensional Modelling Results. *J. Atmos. Chem.* 36, 157–230.
729 doi:10.1023/A:1006300616544
- 730 Quennehen, B., Raut, J.-C., Law, K.S., Ancellet, G., Clerbaux, C., Kim, S.-W., Lund, M.T.,
731 Myhre, G., Olivie, D.J.L., Safieddine, S., Skeie, R.B., Thomas, J.L., Tsyro, S., Bazureau,
732 A., Bellouin, N., Daskalakis, N., Hu, M., Kanakidou, M., Klimont, Z., Kupiainen, K.,
733 Myriokefalitakis, S., Quaas, J., Rumbold, S.T., Schulz, M., Cherian, R., Shimizu, A., Wang,
734 J., Yoon, S.-C., Zhu, T., 2015. Multi-model evaluation of short-lived pollutant distributions
735 over East Asia during summer 2008. *Atmos. Chem. Phys. Discuss.* 15, 11049–11109.
736 doi:10.5194/acpd-15-11049-2015
- 737 Russell, G.L., Lerner, J.A., 1981. A New Finite-Differencing Scheme for the Tracer Transport
738 Equation. *J. Appl. Meteorol.* 20, 1483–1498. doi:10.1175/1520-
739 0450(1981)020<1483:ANFDSF>2.0.CO;2
- 740 Sciare, J., Oikonomou, K., Favez, O., Liakakou, E., Markaki, Z., Cachier, H., Mihalopoulos, N.,
741 2008. Long-term measurements of carbonaceous aerosols in the Eastern Mediterranean:
742 evidence of long-range transport of biomass burning. *Atmos. Chem. Phys.* 8, 5551–5563.
743 doi:10.5194/acp-8-5551-2008
- 744 Stevenson, D.S., Dentener, F.J., Schultz, M.G., Ellingsen, K., van Noije, T.P.C., Wild, O., Zeng,
745 G., Amann, M., Atherton, C.S., Bell, N., Bergmann, D.J., Bey, I., Butler, T., Cofala, J.,
746 Collins, W.J., Derwent, R.G., Doherty, R.M., Drevet, J., Eskes, H.J., Fiore, a. M., Gauss,
747 M., Hauglustaine, D. a., Horowitz, L.W., Isaksen, I.S. a., Krol, M.C., Lamarque, J.-F.F.,
748 Lawrence, M.G., Montanaro, V., Müller, J.-F.F., Pitari, G., Prather, M.J., Pyle, J. a., Rast,
749 S., Rodriguez, J.M., Sanderson, M.G., Savage, N.H., Shindell, D.T., Strahan, S.E., Sudo,
750 K., Szopa, S., 2006. Multimodel ensemble simulations of present-day and near-future
751 tropospheric ozone. *J. Geophys. Res.* 111, D08301. doi:10.1029/2005jd006338
- 752 Stohl, A., Aamaas, B., Amann, M., Baker, L.H., Bellouin, N., Berntsen, T.K., Boucher, O.,
753 Cherian, R., Collins, W., Daskalakis, N., Dusinska, M., Eckhardt, S., Fuglestvedt, J.S.,
754 Harju, M., Heyes, C., Hodnebrog, Ø., Hao, J., Im, U., Kanakidou, M., Klimont, Z.,
755 Kupiainen, K., Law, K.S., Lund, M.T., Maas, R., MacIntosh, C.R., Myhre, G.,
756 Myriokefalitakis, S., Olivie, D., Quaas, J., Quennehen, B., Raut, J.-C., Rumbold, S.T.,
757 Samset, B.H., Schulz, M., Seland, Ø., Shine, K.P., Skeie, R.B., Wang, S., Yttri, K.E., Zhu,
758 T., 2015. Evaluating the climate and air quality impacts of short-lived pollutants. *Atmos.*
759 *Chem. Phys. Discuss.* 15, 15155–15241. doi:doi:10.5194/acpd-15-15155-2015
- 760 Tiedtke, M., 1989. A Comprehensive Mass Flux Scheme for Cumulus Parameterization in
761 Large-Scale Models. *Mon. Weather Rev.* 117, 1779–1800. doi:10.1175/1520-
762 0493(1989)117<1779:ACMFSF>2.0.CO;2
- 763 van der A, R.J., Allaart, M. a. F., Eskes, H.J., 2010. Multi sensor reanalysis of total ozone.

764 Atmos. Chem. Phys. 10, 11277–11294. doi:10.5194/acp-10-11277-2010

765 van Noije, T.P.C., Eskes, H.J., van Weele, M., van Velthoven, P.F.J., 2004. Implications of the
766 enhanced Brewer-Dobson circulation in European Centre for Medium-Range Weather
767 Forecasts reanalysis ERA-40 for the stratosphere-troposphere exchange of ozone in global
768 chemistry transport models. *J. Geophys. Res.* 109, D19308. doi:10.1029/2004JD004586

769 Voulgarakis, A., Naik, V., Lamarque, J.-F., Shindell, D.T., Young, P.J., Prather, M.J., Wild, O.,
770 Field, R.D., Bergmann, D., Cameron-Smith, P., Cionni, I., Collins, W.J., Dalsøren, S.B.,
771 Doherty, R.M., Eyring, V., Faluvegi, G., Folberth, G.A., Horowitz, L.W., Josse, B.,
772 MacKenzie, I.A., Nagashima, T., Plummer, D.A., Righi, M., Rumbold, S.T., Stevenson,
773 D.S., Strode, S. a., Sudo, K., Szopa, S., Zeng, G., 2013. Analysis of present day and future
774 OH and methane lifetime in the ACCMIP simulations. *Atmos. Chem. Phys.* 13, 2563–2587.
775 doi:10.5194/acp-13-2563-2013

776 Voulgarakis, A., Telford, P.J., Aghedo, a. M., Braesicke, P., Faluvegi, G., Abraham, N.L.,
777 Bowman, K.W., Pyle, J. a., Shindell, D.T., 2011. Global multi-year O₃-CO correlation
778 patterns from models and TES satellite observations. *Atmos. Chem. Phys.* 11, 5819–5838.
779 doi:10.5194/acp-11-5819-2011

780 Yue, X., Unger, N., 2014. Ozone vegetation damage effects on gross primary productivity in the
781 United States. *Atmos. Chem. Phys.* 14, 9137–9153. doi:10.5194/acp-14-9137-2014

782 Zanis, P., Hadjinicolaou, P., Pozzer, A., Tyrlis, E., Dafka, S., Mihalopoulos, N., Lelieveld, J.,
783 2014. Summertime free-tropospheric ozone pool over the eastern Mediterranean/Middle
784 East. *Atmos. Chem. Phys.* 14, 115–132. doi:10.5194/acp-14-115-2014

785

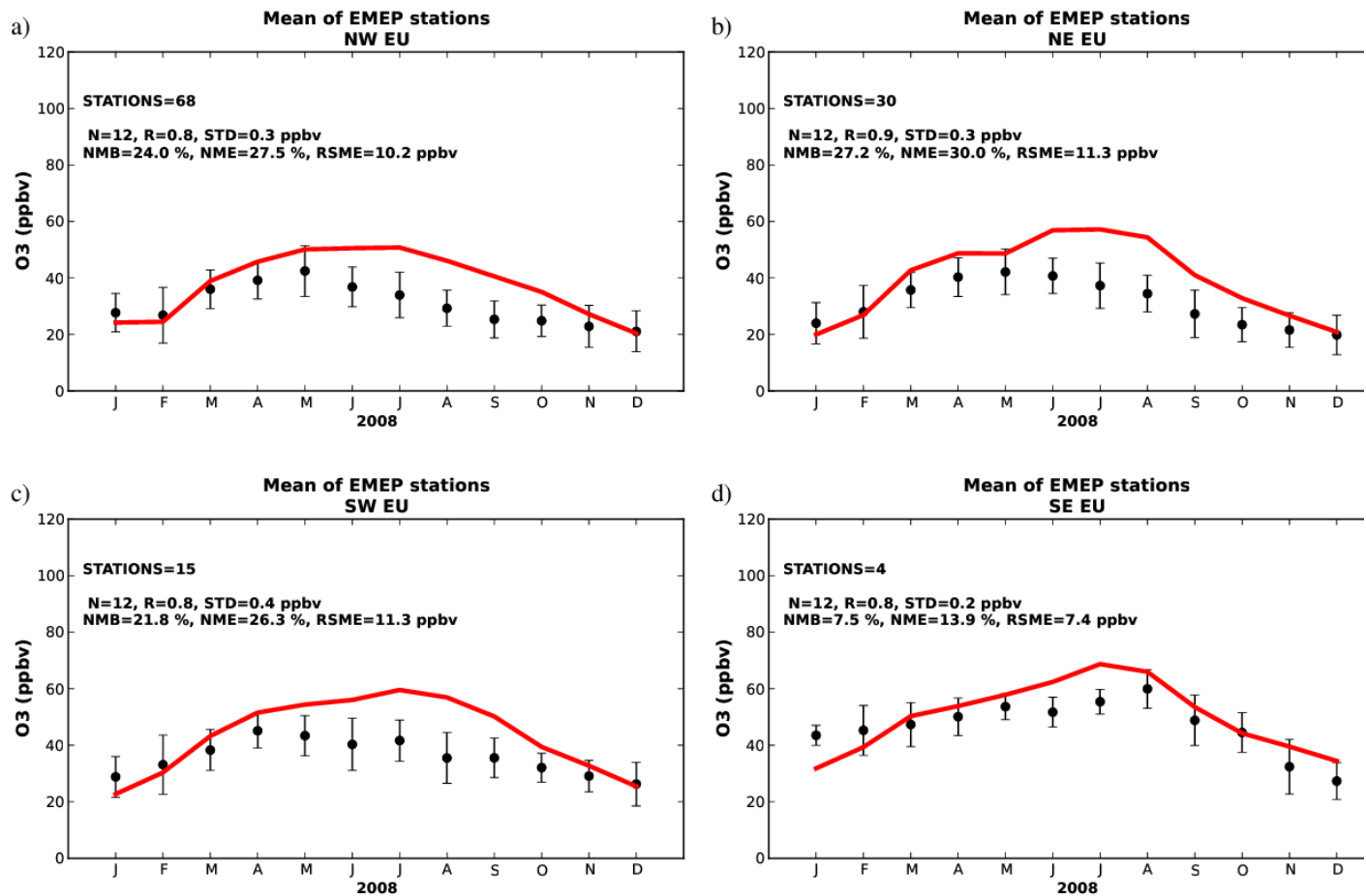
786

787 **Table 1.** Outline of simulations performed for this study.

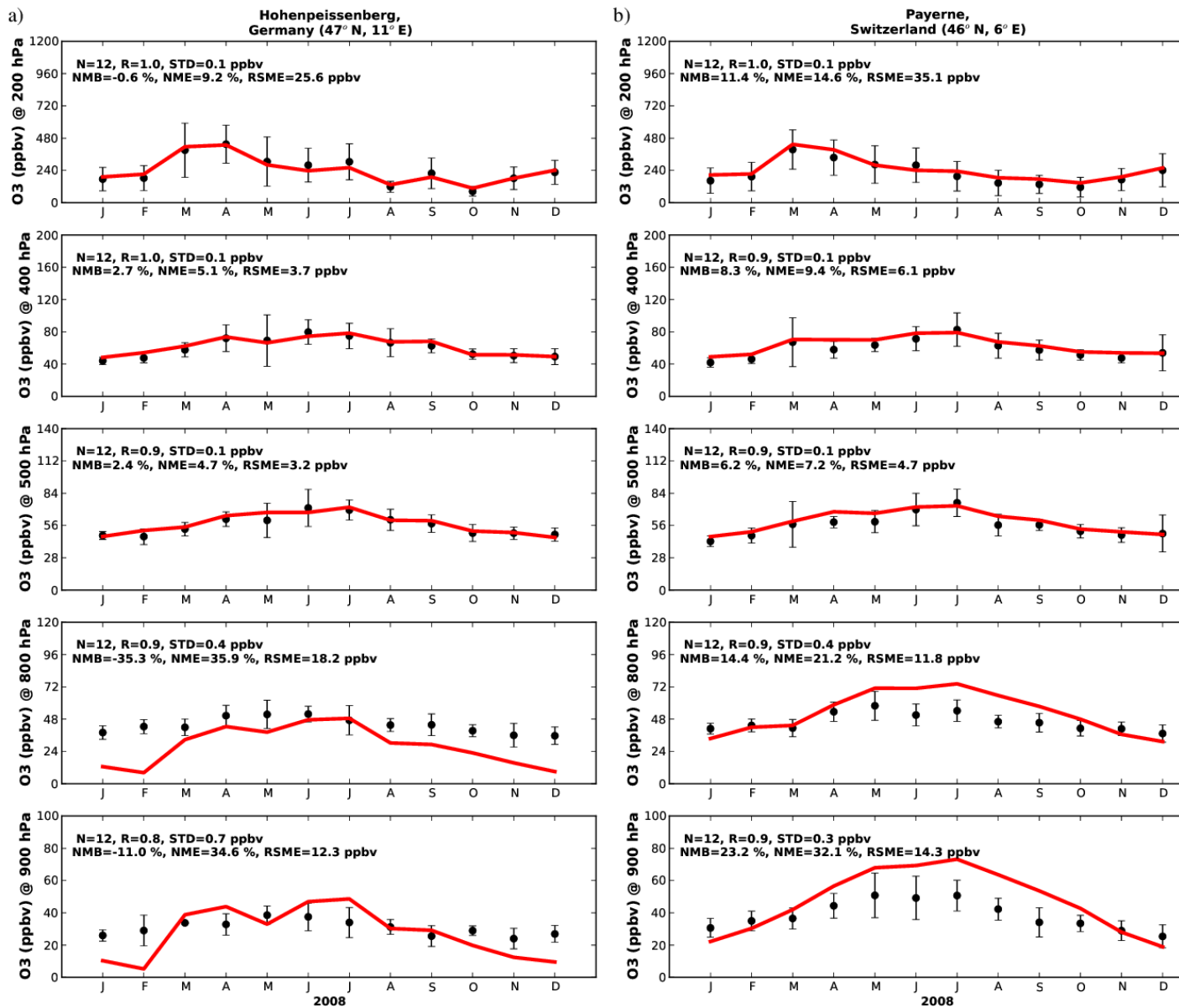
Simulation	Description
BASE	The base case simulation for the year 2008.
MaskANTRO	Neglecting the anthropogenic emissions in the Eastern Mediterranean domain.
MaskBB	Neglecting the biomass burning emissions in the Eastern Mediterranean domain.
MaskBIO	Neglecting the biogenic emissions in the Eastern Mediterranean domain.
MaskALL	Neglecting the anthropogenic, biomass burning and biogenic emissions in the Eastern Mediterranean domain.
MaskEU	Neglecting all emissions over Europe.
MaskNAM	Neglecting all emissions over Northern America.
MaskAS	Neglecting all emissions over Asia.
MaskAF	Neglecting all emissions over Africa.
FUTURE	Taking into account projected anthropogenic emission of the year 2050.

788

789



790
 791 **Fig. 1.** Comparison of O₃ levels (ppb_v) from TM4-ECPL BASE simulation (red lines) with
 792 surface monthly mean observations from EMEP stations (black dots) and the respective standard
 793 deviation of the observed O₃ levels (ppb_v) (with black vertical lines) at a) NW Europe, b) NE
 794 Europe, c) SW Europe and d) SE Europe.
 795



796

797

798

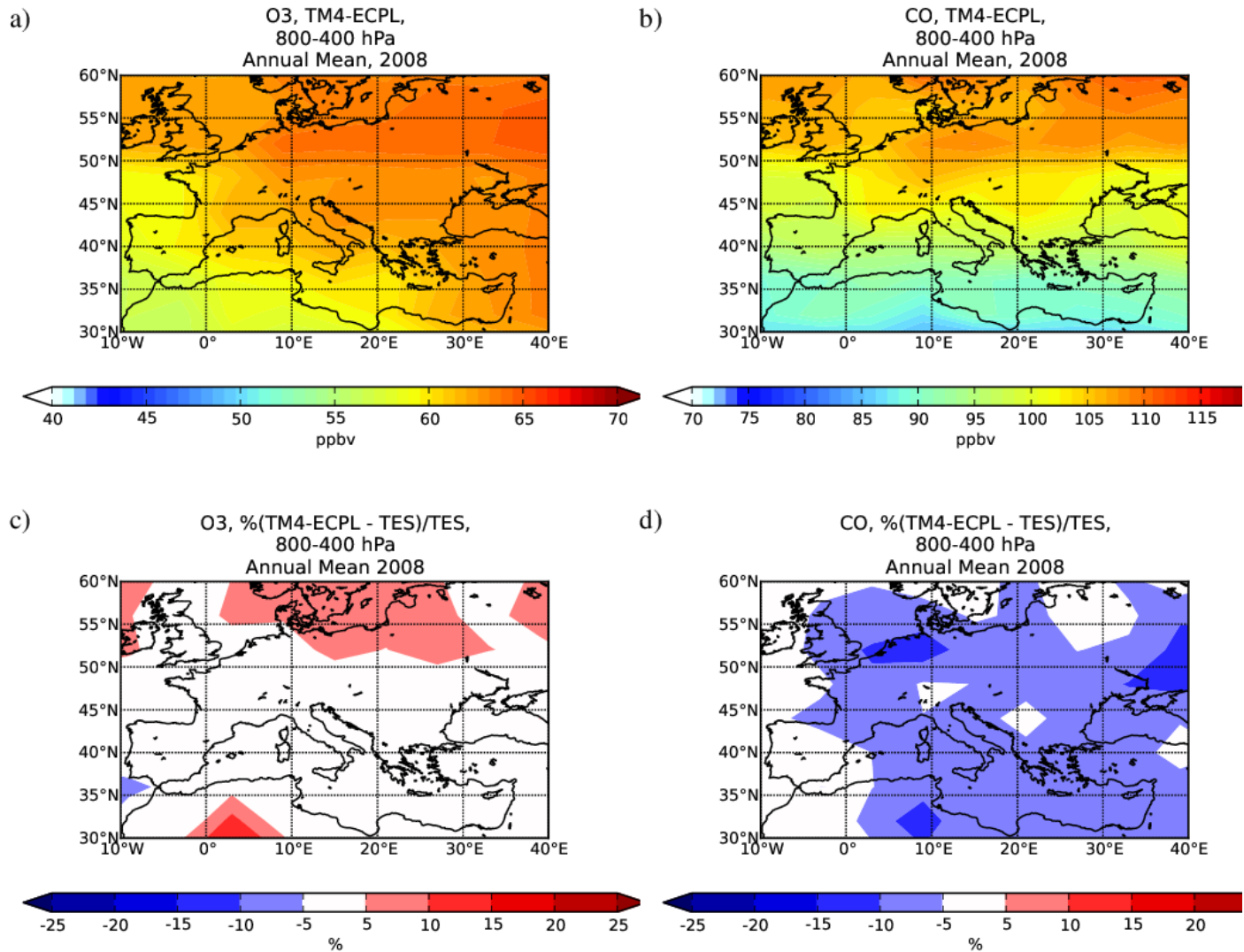
799

800

801

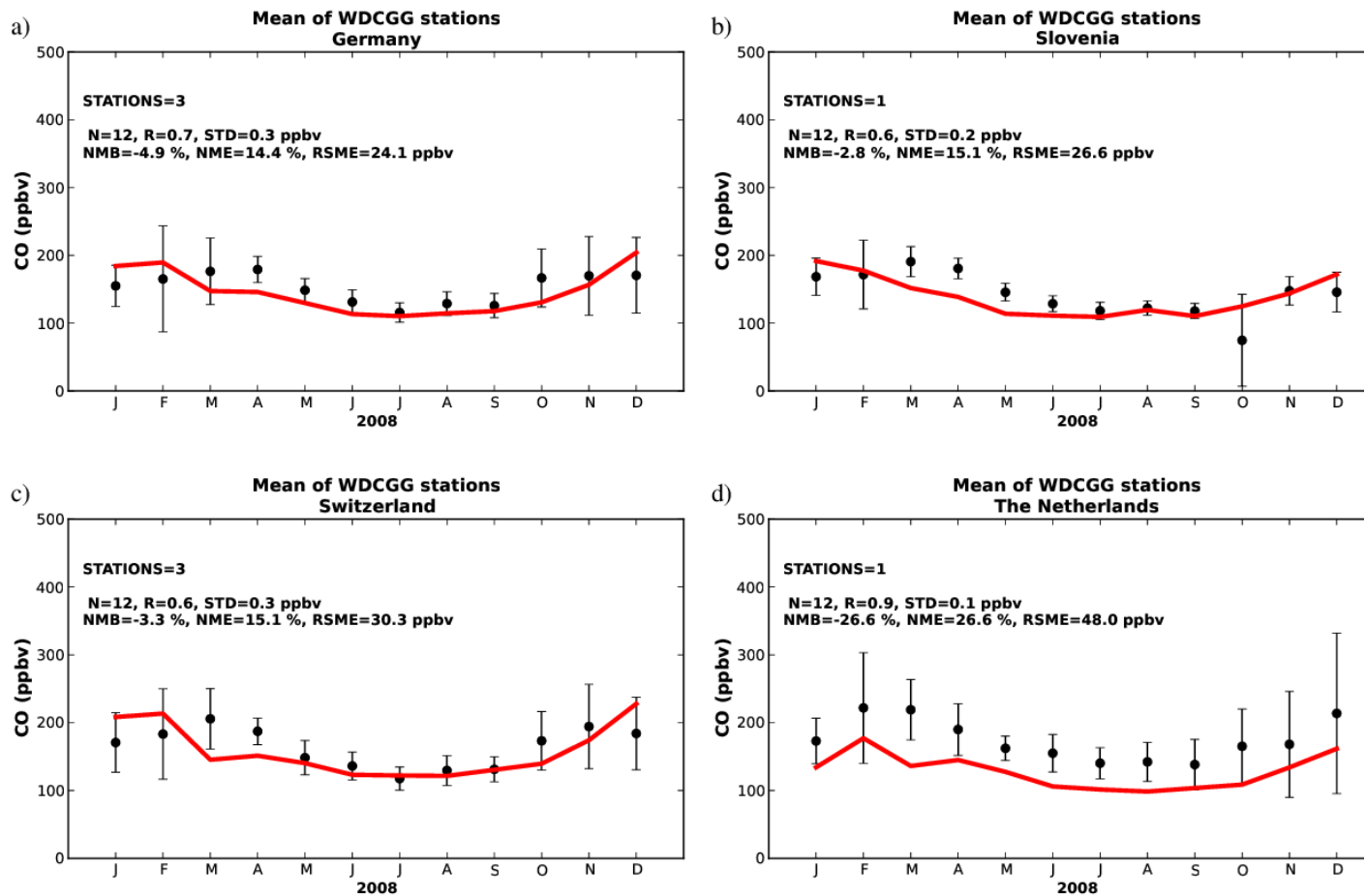
Fig. 2. Comparison of O₃ levels (ppbv) from TM4-ECPL BASE simulation (red line) with O₃ sonde station data (black dots, mean and standard deviation) at five pressure levels (900; 800; 500; 400; 200 hPa) for two WOUDC stations: a) Hohenpeissenberg, Germany (47°N, 11°E); b) Payerne, Switzerland (46°N, 6°E) (see additional comparisons at other European stations in Fig. S3 in the supplementary material).

802



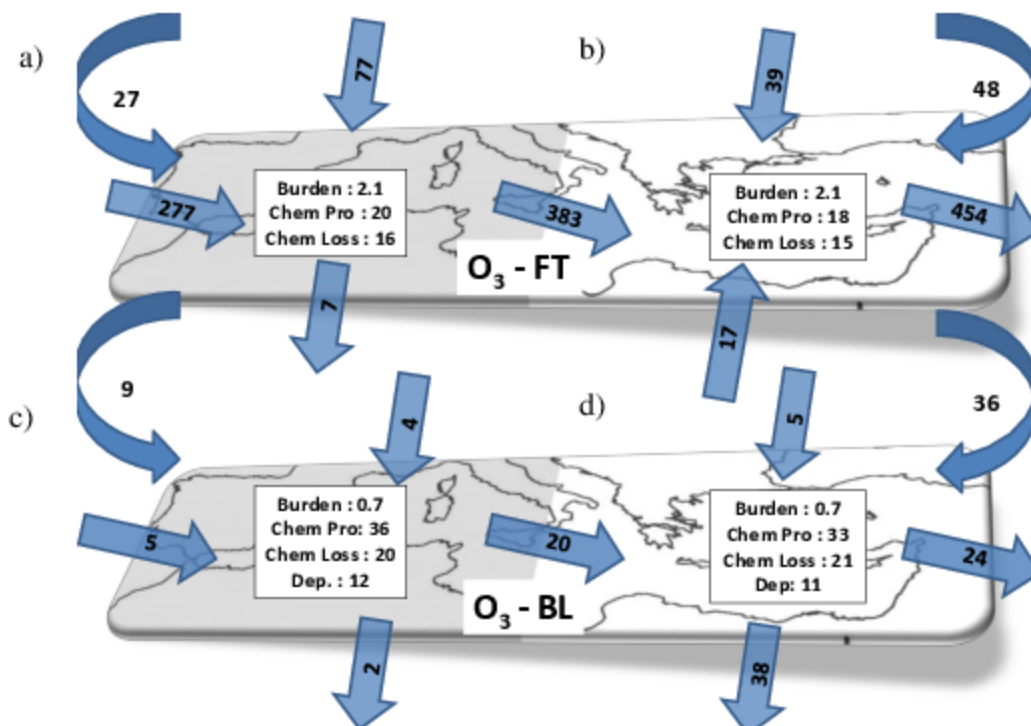
803
 804 **Fig. 3.** Simulated annual mean free tropospheric concentrations (ppbv) in the 800-400 hPa zone
 805 over Europe for a) O₃, b) CO, and the percentage difference of TM4-ECPL BASE simulation
 806 results from TES retrieved concentrations [100 x (BASE-TES)/TES] for c) O₃ and d) CO in the
 807 same zone.

808

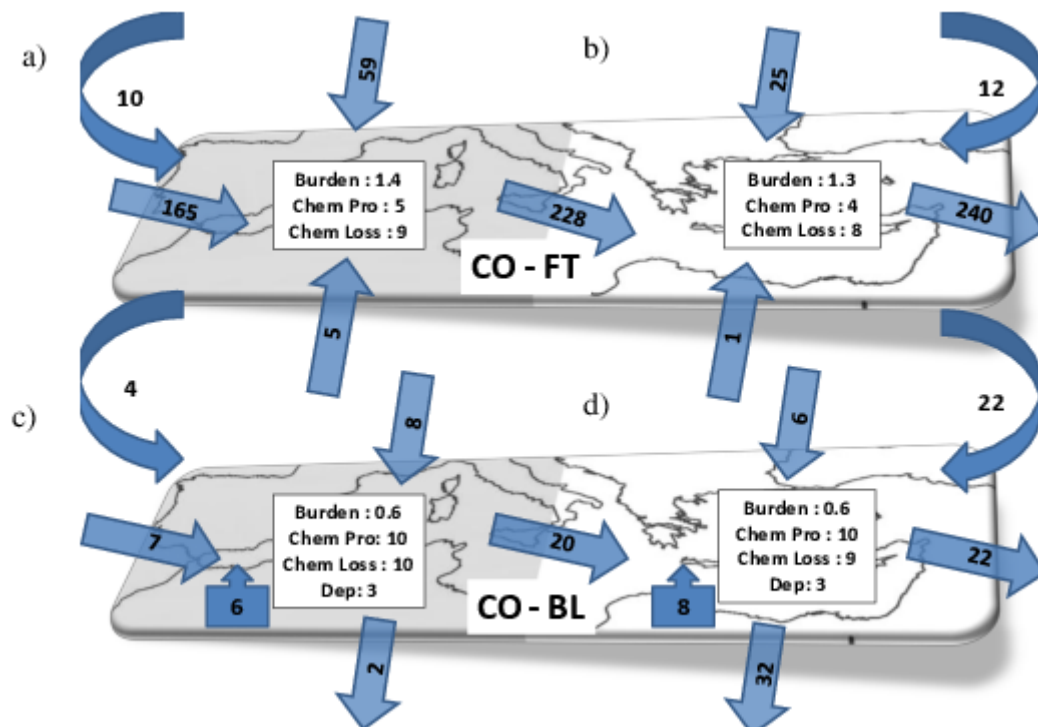


809
 810 **Fig. 4.** Comparison of surface CO levels (ppbv) calculated by TM4-ECPL BASE simulation (red
 811 line) with observations (monthly mean values for WDCGG stations, black dots, mean and
 812 standard deviation) at a) Germany, b) Slovenia c) Switzerland and d) The Netherlands

813

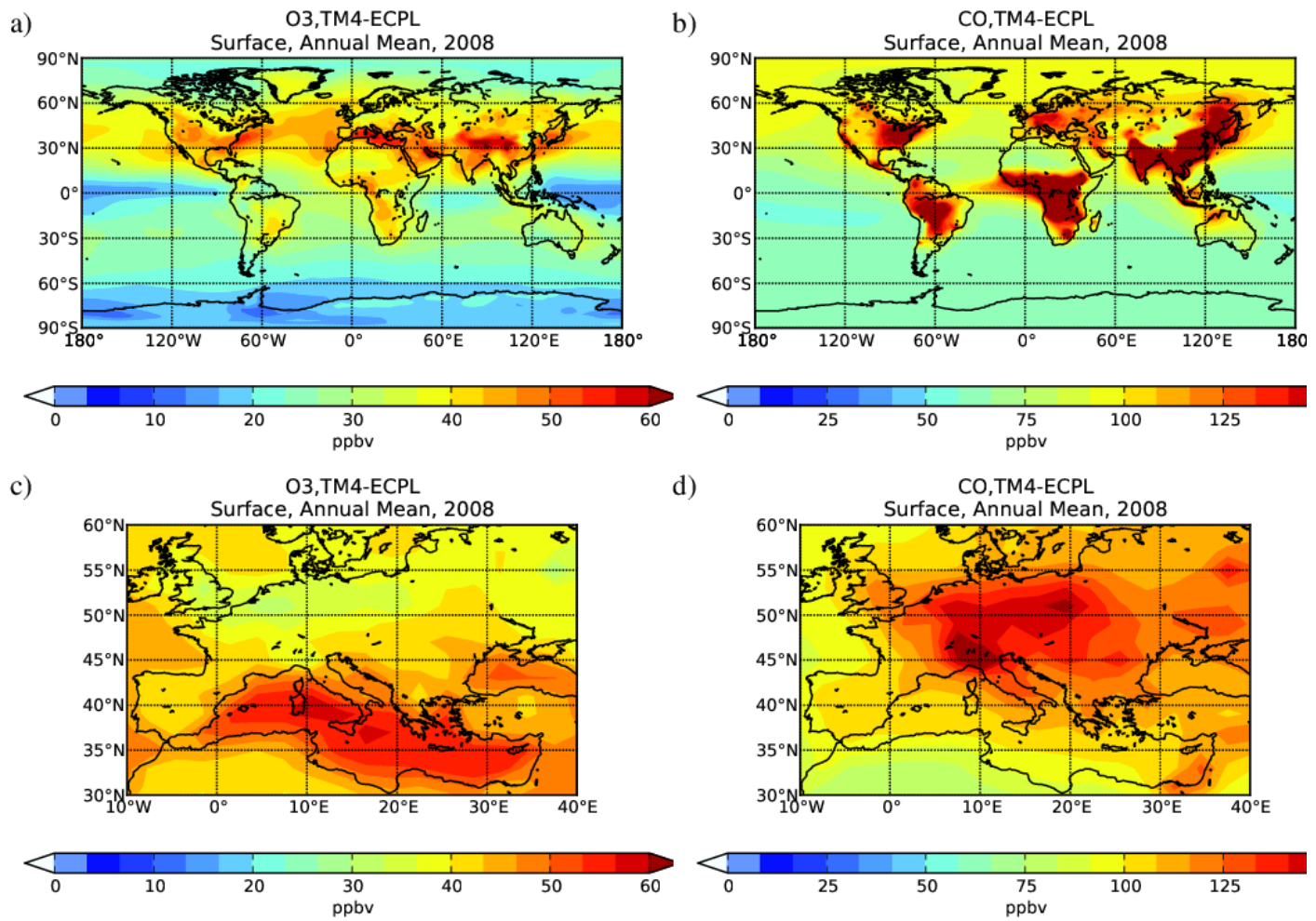


814
 815 **Fig. 5.** O₃ annual (2008; BASE simulation) budget analysis for Western (a,c; shaded area) and
 816 Eastern Mediterranean (b,d; non-shaded area) for a,b) the free troposphere (FT; upper figure) and
 817 c,d) the boundary layer (BL; bottom figure) including the burden, the chemistry, the deposition
 818 and the fluxes at each boundary. All budget terms and fluxes (Tg yr⁻¹) are annual totals; burdens
 819 (Tg) are annual averages. Straight arrows indicate N-S and W-E advection fluxes, while curved
 820 arrows indicate vertical fluxes from the upper troposphere to the FT and from the FT to the BL.
 821



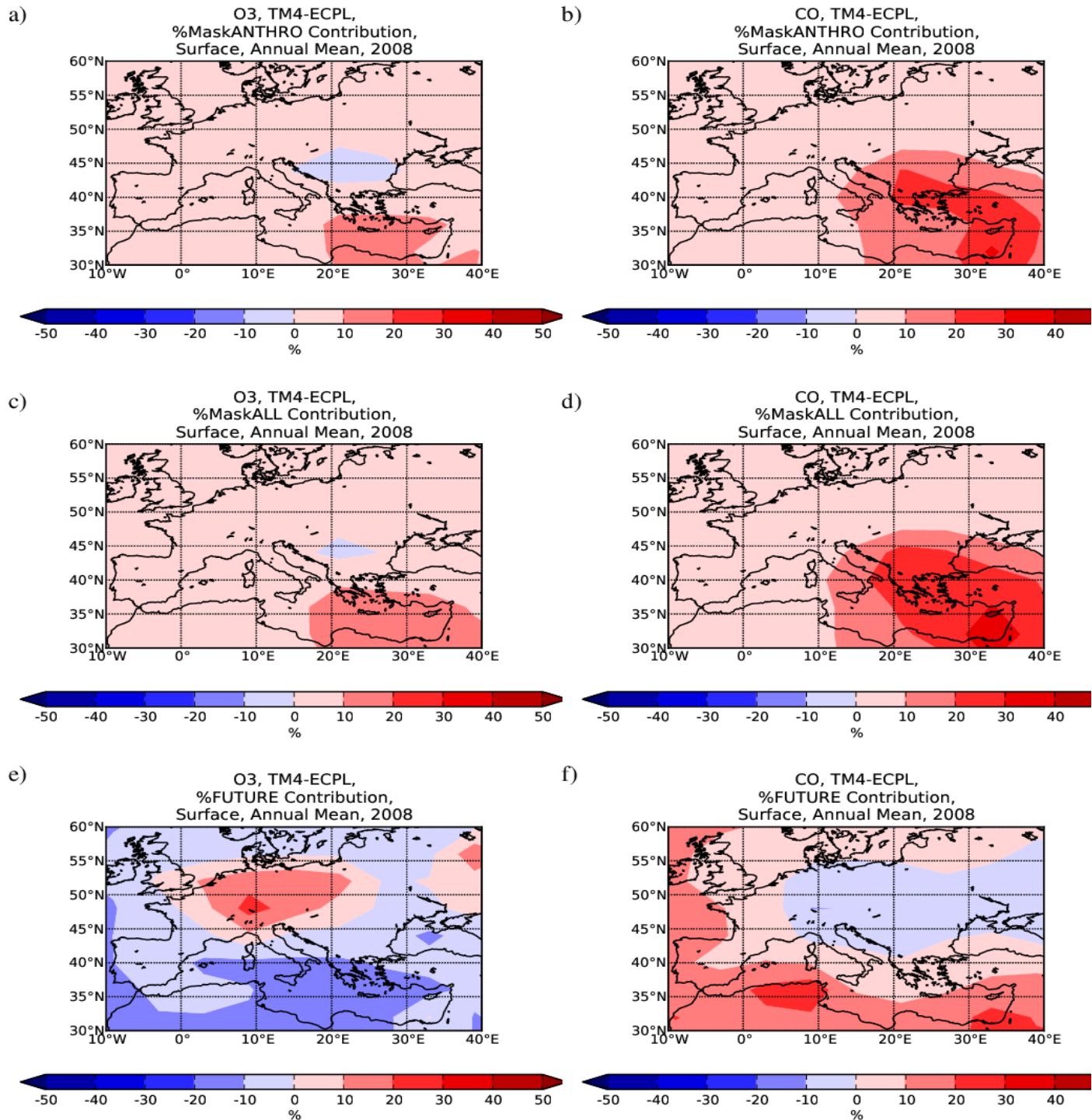
822
 823 **Fig. 6.** CO annual (2008; BASE simulation) budget analysis for Western (a,c; shaded area) and
 824 Eastern Mediterranean (b,d; non-shaded area) for a,b) the free troposphere (FT; upper figure) and
 825 c,d) the boundary layer (BL; bottom figure) including the burden, the emissions, the chemistry,
 826 the deposition and the fluxes at each boundary.. Straight arrows indicate N-S and W-E advection
 827 fluxes, curved arrows indicate vertical fluxes from the upper troposphere to the FT and from the
 828 FT to the BL and box-arrows indicate CO emissions.

829
 830
 831



832
 833
 834
 835

Fig. 7. Simulated a,c) O₃ and b,d) CO surface concentrations (ppb_v) for TM4-ECPL BASE simulation for the globe (a,b) and focus on the Mediterranean area (c,d).



837
 838 **Fig. 8.** Simulated relative contribution (%) to O₃ (left panels) and CO (right panels) surface
 839 concentrations of a,b) Anthropogenic emissions over EM (MaskANTHRO); c,d) All emissions
 840 over the EM (MaskALL); and e,f) Future anthropogenic emissions (FUTURE), compared to the
 841 TM4-ECPL BASE simulation (figures a) through d) are computed as $[100 \cdot (\text{BASE} -$
 842 $\text{MaskX}) / \text{BASE}]$; where MaskX is the respective sensitivity simulation, while e) and f)
 843 are computed as $[100 \cdot (\text{FUTURE} - \text{BASE}) / \text{BASE}]$.
 844